ADVANCED SUSTAINABLE SYSTEMS
www.advsustainsys.com

Immobilized Molecular Catalysts for CO_2 Photoreduction

Mar Reguero, Carmen Claver, Rui Miguel Barroso Carrilho, and Anna Maria Masdeu-Bultó**

Catalytic carbon dioxide transformation to low valence carbon molecules such as carbon monoxide, formic acid, methanol and methane is a sustainable way to produce fuels and chemicals. Molecular catalysts can be designed to selectively transform CO_2 at mild conditions, but a solvent medium is required. Instead, the molecular catalysts can be immobilized on solid supports to facilitate the continuous flow procedure and the separation of the products to recycle the catalytic systems for a more sustainable process. Photosensitive supports may also favor the light-absorbing steps and electron transfer processes. In this article, the recent results obtained in the photocatalytic CO_2-reduction using catalytic systems formed by molecular compounds anchored on solids are reviewed.

1. Introduction

Carbon dioxide, CO_2, is the product of the aerobic combustion of carbon-containing reagents. As such, large amounts of CO_2 are generated by human activities mainly by the burning of fossil fuels to obtain energy for transport and industrial production. These anthropogenic emissions are estimated to be of the order of 35 Gt of CO_2 per year, part of which has accumulated in the atmosphere, reaching a concentration of more than 400 ppm.[1] CO_2 is one of the gases that generates the greenhouse effect, so the increase in its concentration is considered to contribute to climate change, what has led to an increase in the global temperature of the planet. Recent climate summits (Kyoto 1992, Paris 2015, Chile-Madrid 2019, and the Glasgow Climate Change conference 2021) have concluded that carbon dioxide emissions should be reduced by 45% by 2030 and reach net zero by 2050 to limit global warming to 1.5 °C.[2] Achieving this goal requires a combination of efforts in different areas.

Therefore, it is essential to develop efficient strategies that led to an effective reduction in carbon dioxide emissions. A complementary approach could be the capture of the carbon dioxide emitted in combustion processes to balance emissions and use it for chemical synthesis. The capture and use of CO_2 (CCU) is an area in fast development due to the high research interest on this topic which has grown exponentially in recent years.[3,4] Especially challenging is the transformation of CO_2 into chemicals[5–11] and fuels.[12,13] This is a very attractive idea, as carbon dioxide can be a low-cost and abundant carbon source for all carbon-based materials. However, CO_2 is a very stable molecule ($\Delta G_f^0 = -394.228$ kJ mol^{-1})[14] since carbon is at its most stable valence (IV), so to transform CO_2 into other products, catalysts and/or highly reactive substances must be used.

The direct reduction of CO_2 to give $CO_2^{\bullet-}$ is an unfavorable process with a formal reduction potential of –1.90 V. Fortunately, proton-assisted electron transfer (PAET) is a more favorable process that can give place to multiple reductions of CO_2 leading to several different products like CO, HCOOH, HCHO, CH_3OH, C_2H_4, or CH_4 with similar reduction potentials varying between –0.24 and –0.61 V as shown in **Table 1**.

Despite the more favorable thermodynamics of these processes, the large stability of CO_2 makes the barriers for any reaction of this compound very high, so for its transformation, it is necessary a significant energy input and the use of efficient catalysts. The most common ways to tackle this challenge are the electrochemical, photochemical, or photoelectrochemical approaches. Combined photoelectrochemical catalytic systems in which semiconductors are used as photoelectrodes and molecular complexes act as catalysts have been also reported,[17–19] but the photochemical approach seems to be more attractive due to the possibility of using directly the green, renewable and powerful source of energy provided by the sun. Nature, through plants and organisms, has harvested sunlight energy for billions of years and used it to synthesize O_2 and carbohydrates from CO_2 and H_2O. In this way, solar energy is efficiently stored in chemicals.[20] In natural photosynthesis, the photosynthetic efficiency for the solar-to-biomass conversion has been estimated to be up to 6.3% for algae, 1–2% for crops, and less than 0.1% for most of the plants[21–23] since not all the visible light range is absorbed and there are energy losses through light dispersion or to prevent photodamage.[24] The artificial photosynthesis devices are designed to enlarge the range of light absorption and some examples are achieving

M. Reguero, C. Claver, A. M. Masdeu-Bultó
Department of Physical and Inorganic Chemistry
Universitat Rovira i Virgili
Carrer Marcel·lí Domingo, 1. Campus Sescelades, Tarragona 43007, Spain
E-mail: annamaria.masdeu@urv.cat
R. M. B. Carrilho
Coimbra Chemistry Centre
Department of Chemistry
University of Coimbra
Rua Larga, Coimbra 3004-535, Portugal
E-mail: rui.carrilho@uc.pt
The ORCID identification number(s) for the author(s) of this article can be found under https://doi.org/10.1002/adsu.202100493.

DOI: 10.1002/adsu.202100493

Table 1. Reduction potentials versus NHE for some reactions of CO_2 in aqueous media.[15,16]

Reduction reaction[a)]	ε^0 [V]
$CO_2 + 0\ H^+ + 1\ e^- \rightarrow CO_2^{\bullet-}$	−1.90
$2CO_2 + 0\ H+ + 2\ e^- \rightarrow C_2O_4^{2-}$	−0.59
$CO_2 + 2\ H^+ + 2\ e^- \rightarrow HCOOH$	−0.61
$CO_2 + 2\ H^+ + 2\ e^- \rightarrow CO + 1\ H_2O$	−0.53
$CO_2 + 4\ H^+ + 4\ e^- \rightarrow HCHO + 1\ H_2O$	−0.48
$CO_2 + 6\ H^+ + 6\ e^- \rightarrow CH_3OH + 1\ H_2O$	−0.38
$CO_2 + 8\ H^+ + 8\ e^- \rightarrow CH_4 + 2\ H_2O$	−0.24

[a)]NHE: potential respect to the normalized hydrogen electrode.

higher efficiencies than the natural photosynthesis systems (>10% for solar-to-hydrogen).[25,26]

Given their advantages and interesting possibilities, the scope of this review is centered on the photocatalytic systems consisting of molecular catalysts supported on solid materials, paying special attention to the metal complexes and their coordination environments.

The main families of catalysts used for photoreduction of CO_2 are metal oxides, inorganic semiconductors,[27,28] metal–organic frameworks, (MOFs),[29,30] molecular catalysts, and hybrid semiconductor with molecular catalysts.[31] Also, photobiocatalytic systems combining semiconductors and enzymes have been reported for CO_2 reduction but enzyme-based catalysts are more selective but less stable under catalytic conditions.[17,32] Metal oxide semiconductors are often highly stable under catalytic conditions but present poor selectivity due to the competitive hydrogen evolution. Most common metal oxides used, such as TiO_2, ZnO, and ZrO_2, have poor absorption in the visible range, so they have to be sensitized or doped to increase the absorbance.[33]

Metal complexes[34–36] are predominant molecular catalysts in the studies of photocatalytic CO_2 reduction due to the clear advantages they present. The transition metals in which they are based can present different oxidation states, what promote PAET reactions and their metal centers are active sites for CO_2 coordination. Metal complexes, such as rhenium(I) bipyridine derivatives are efficient in light absorption in the visible range[37] and their properties (including stability, redox potentials, inductive, and steric effects) can be tuned by modification of the ligands and consequently their reactivity can be controlled. This characteristic is very important given that selectivity is a crucial issue in this process, due to the similar reduction potentials of the reactions to obtain different products from CO_2 and the modulation of the catalyst reactivity is essential to improve its performance. Another attractive characteristic of these catalysts is that their molecular structure is well determined. This fact facilitates mechanistic studies that can give information about the relationship between structure and performance what would eventually help in the endeavor of designing better catalysts.

But these molecular catalysts are not free from drawbacks. The capacity of light absorption makes them prone to suffer photo-dissociation or photo-isomerization reactions, so they are not robust systems. On top of that, being homogenous catalysts, their recyclability is not easy. This issue, together with the generalized use of noble and rare metals makes them expensive and not convenient from the environmental point of view. This problem is worsened by the fact that these catalysts, in many cases, need to work together with a photosensitizer, usually also based on noble metals, and a sacrificial electron donor. Recently, many efforts are oriented to use earth-abundant cheap non-noble metals in photocatalytic systems for CO_2 reduction and sustainable related processes such as water splitting[38] and artificial photosynthesis.[39]

Heterogenous catalysts are mainly based on semiconductors or composites. Numerous studies are based on TiO_2 derivatives, but ZrO_2 is also used frequently together with other metal sulfides or oxonitrides.[40–42] Carbon-based nanocomposites have also shown great potential as catalysts for CO_2 photoreduction.[43,44] Under photoexcitation, these materials promote electrons to the conduction band, which are available to reduce CO_2. These heterogenous catalysts have the advantages of being more robust under the reaction conditions and easily recovered and recycled. On the other hand, they have the drawback of being little efficient under sunlight because their absorbance is mainly in the UV range, due to the usually large gap between valence and conduction bands. On top of this, their quantum efficiency is low and their selectivity is poor. Nevertheless, research conducted on tuning these kinds of systems is expected to allow to overcome or mitigate these problems and make of nanocomposites interesting photochemical catalysts. Better performances are shown by functionalized covalent organic polymers,[45,46] but in all cases, there is ample room for improvement.

The use of MOFs for the catalysis of CO_2 reduction reactions has recently experienced rapid development.[47–49] The capacity of adsorption of CO_2 and the large number of catalytic sites (due to their porosity and large surface) of these materials make them very interesting and promising systems. Another attractive characteristic is the possibility of modifying their structure to tune their light-harvesting properties and pore size while keeping it uniform. Unfortunately, they not always are stable under reaction conditions.

The landscape on homogenous as well as on heterogenous catalysis shows that, although there have been good achievements so far in some cases, the catalytic systems developed up to now are not free from problems.

A strategy to overcome the drawbacks of the molecular catalysts, which are the ones that in general show better yields and selectivity, is to heterogenize them, anchoring them to some kind of support. If the support is not a passive spectator, it can contribute in one way or another in the catalysis in such a way that it does not only improve the catalytic system due to the combination of the advantages of homogenous and heterogenous catalysts but also enhances the performance due to the synergy between the activities of the molecular complex and the support. The success of this approach has been demonstrated, e.g., in the high activity and selectivity obtained in the photoreduction of CO_2 to formic acid, achieved by hybrid catalytic systems containing ruthenium complexes anchored in Ag-nanoparticles on graphitic carbon nitride support.[50]

The main advantage of heterogenized systems over semiconductor-based ones is that in the first type, the molecular component can be designed to tune the catalytic activity by ligands' modifications and they can be tested separately. In semiconductor-based photocatalysts, it is often difficult to control the photogenerated charge carriers and surface reactions due to

the multiple active sites that may be present, thus leading to less selective systems.[51] Also some of the best-suited oxides for photoreduction such as Cu_2O, CdS, GaP, TaON, C_3N_4, and Ta_3N_5 present low photostability. Furthermore, semiconductor-based systems require high purity materials of high cost, that tend to degrade under prolonged operation in electrolyte solutions.[23] In any case, both approaches are still far from the optimized conditions and should be further developed.

The molecular catalysts and support materials that have been used following the strategy of heterogenization show a large variety, and in this sense, it would be interesting to have a global picture of the development of these supported catalysts. This review presents a systematic compilation of a wide range of examples of the efforts made in this sense to help to further advance in this line of research. We expect that it will aid in the fight against anthropogenic CO_2 atmospheric pollution.

In the next section, we provide basic information about the reactivity of carbon dioxide and describe the general mechanism of the photocatalytic reduction of CO_2. The different steps of this mechanism justify the need for the different components of the catalytic systems for this reaction and explain the possible contribution of supports to the catalytic activity. In the following sections, an extensive selection of examples of supported catalysts for CO_2 photoreduction is presented. It has been organized in different sections according to the type of ligand of the molecular catalyst used. This criterion was chosen considering that the coordination environment of the molecular catalyst is crucial from the point of view of the chemical reactivity, due to the importance of the electronic and steric properties of the ligands, influencing both activity and selectivity. Furthermore, ligand modification synthesis determines the way of anchoring the catalyst to the solid support. Thus, polypyridyl, cyclam, and tetrapyrrole-based complexes are discussed. The paper ends with the conclusions and an outlook drawn from the global scenario depicted in the previous section.

2. Background and General Mechanism of CO_2 Photocatalytic Reduction and Its Implications

As already mentioned, the CO_2 molecule is practically inert. The main exceptions regarding its reactivity are related to its acid–base behavior and its ability to interact with transition metals, properties that can be explained based on its molecular orbitals HOMO (highest occupied molecular orbital) and LUMO (lowest unoccupied molecular orbital). The first one is a doubly occupied $1\Pi_g$ orbital, located mainly on the oxygen atoms, that consequently show a Lewis base character. On the other hand, the $2\Pi_u$ LUMO is concentrated around the central carbon, providing it with the characteristics of a Lewis acid. Globally, therefore, CO_2 has an amphoteric character. However, CO_2 is a better acceptor of charge density, given that the electrophilic character of carbon predominates over the nucleophilic behavior of oxygen.[52]

This amphoteric character also allows CO_2 to bind with electron-rich and electron-poor catalytic sites, and the activation of CO_2 by coordination with the metal center can take place in different ways. The most common coordination mode is η^2-C,O "side on" type. This type of interaction can be described as the formation of the bond by donation of the electrons centered on one of the oxygen atoms ($1\Pi_g$) with an important contribution by back donation of d-electrons of the metal to the empty orbital $2\Pi_u$ centered on the C atom.[52] That is, CO_2 acts as both an electron donor and acceptor.

When CO_2 is coordinated to metals with marked nucleophilic character, a η^1-CO_2 binding mode is established. Here, the main contribution to the coordination is the transference of the d-electrons of the metal to the empty CO_2 LUMO. When CO_2 interacts with a surface or with molecular complexes with several metal centers, a η^2-O,O coordination pattern can be found, where both oxygen atoms interact with the catalyst. The η^1-OCO "end-on" approaching mode is very rare, and its interest is almost exclusively theoretical.

In the first three cases, CO_2 undergoes a distortion of the linearity and the nucleophilic character of the oxygen atoms is modified. When CO_2 bends, the energy of the LUMO decreases and the capture of electrons for reduction is favored. This is probably one of the reasons why the η^1-OCO "end-on" coordination, where CO_2 maintains its linearity, is not usual.

The catalyst is the main which is responsible for coordinating CO_2 to activate the molecule and make possible its transformation, but this is not the only step of the reaction of CO_2 reduction. To design better catalysts, we need to know the essential steps of the reaction mechanism to understand how the catalytic system works. Nevertheless, given the complexity of this kind of reactions, to fine-tune a catalyst in a determined process, it is necessary to know the details of each specific case to identify the bottlenecks or rate-determining steps, but these detailed mechanistic studies are out of the scope of this review (for a more specific review on this topic, see ref. [53]).

In photocatalysis, the first step is the light-harvesting that must generate charges. For practical reasons, it is more interesting to maximize light absorption in the visible range to be able to use sunlight as the energy source. In many heterogenous catalysts, the absorption range is given by the energy gap between the valence and conduction band, which can be tuned (by doping or modification of the 3D structure, e.g.) to promote absorption in the desired frequency range. In homogenous catalytic systems, in general, is not the catalyst the species that harvests light, but a photosensitizer that must be part of the system.

The next step is the charge separation (or electron–hole separation). The minimization of the charge recombination is then an essential characteristic to design efficient catalytic systems. In heterogenous catalysts, this separation can be enhanced by polarization caused, e.g., by heterojunctions of polar surface terminators that can channel electrons and holes in different directions. In homogenous catalysts, electron transfer between different components of the system will generate reductive and oxidative species separately, what implies that to design an effective system it is necessary for an adequate fitting between the redox potentials of the different components of the catalytic systems and the substrate.

As commented before, the CO_2 activation is crucial, so the density and efficiency of the activation sites must be optimized. Given that the activation can take place by any of the coordination modes described before, the nature of the activation sites is not unique. In heterogenous catalysts, vacancies on surfaces of extended π-conjugated electronic structures

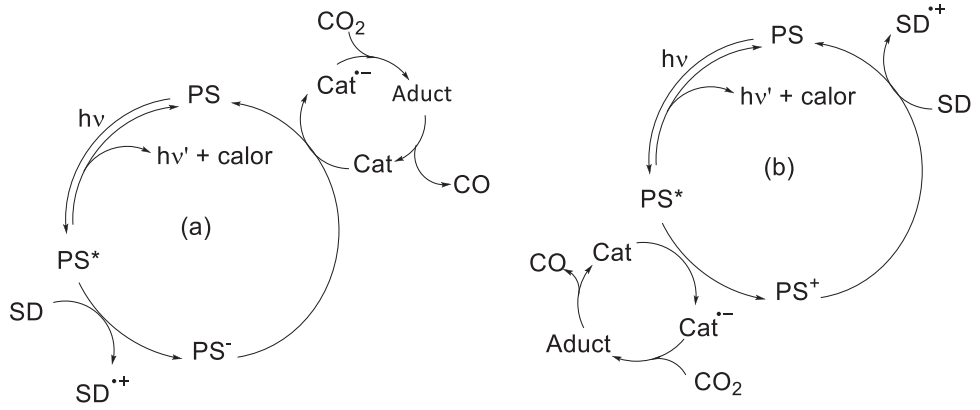

Scheme 1. a) Reductive quenching and b) oxidative quenching in photocatalyzed CO_2 reduction.[15]

can provide efficient adsorption and activation sites. In MOFs and homogenous catalysts, unsaturated metal centers act very often as strong activators, but their ligands can modify their capacity by steric, structural, or electronic effects, preventing or cooperating in the activation.

Finally, the transformation reaction must take place. In this last step, an efficient catalyst must provide the desired product. Given the close similarity between the redox potentials of the different reduction reactions of CO_2 and the competitivity with the reduction reaction of hydrogen, the selectivity is a real issue that makes the difference between potentially efficient catalytic systems. The selectivity is associated with thermodynamic and kinetic factors. The catalytic system used must stabilize intermediates of the expected reaction and desorb products, but also must decrease the barriers of the desired path.

To produce the steps described up to here, the homogenous catalytic systems for the photoreduction of CO_2 are formed typically by a photosensitizer (PS), a sacrificial electron donor (SD), and the catalysts (Cat).

The PS must absorb in the desired wavelength range (preferentially visible) to reach an excited state (PS*) with a long enough lifetime to allow for an electron transfer instead of deexcitation. This can be usually obtained in systems with efficient intersystem crossings that populate triplet states that present long half-live times. Depending on the relative reduction and oxidation potentials of the excited PS, SD, and Cat, the quenching of the PS* will take place by reductive or oxidative processes in a sequence of events shown in **Scheme 1** that give place to the charge separation.

CO_2 must suffer several consecutive proton-assisted reductions. The source of electrons is the sacrificial donor that in many cases is also the source of protons. When water is present in the medium, the provision of protons is easier, but the production of H_2 can affect severely the selectivity of the CO_2 reduction.

The heterogenization of the homogenous catalysts does not modify the stages of the reaction but the support does not, in general, act as a mere spectator. All the opposite, it can enhance the performance of the homogenous catalyst contributing to one or several steps of the reduction reaction. In fact, many examples of this synergy are found in the literature as will be detailed further down. For example, TiO_2 derivatives[54] and carbon-based supports like modified graphene,[55,56] carbon fibers[57] of covalent organic polymers[58] enhance light-harvesting and increase the efficiency of charge separation. The last kind of these mentioned supports are also electron donors, acting in such a way that there is no need for another sacrificial donor, at the same time that they help to adsorb CO_2. This is as well the case of mesoporous materials like silica[59] or zeolite frameworks[60] and MOFs that will help to increase the CO_2 concentration, characteristic especially important in aqueous media given the low solubility of CO_2 in water. These porous materials can also incorporate other guest molecules like PS or Cat.[57,61,62] The proximity of these components of the catalytic system facilitates the electron transfer between them, favoring the kinetics of the reduction reaction. MOFs can also have some specific influence on the catalytic performance given that they can incorporate in the framework any of the components of the catalytic systems, but on top of this they can also have some specific contribution in the catalytic mechanism like the reported inhibition of dimerization of Mn-based catalyst complexes that decrease their efficiency.[63]

As a whole, as it will be exemplified in the next section, the fixation of the homogenous catalyst in heterogenous substrates does not only improve their stability and allow recycling (making these systems more sustainable), but also can enhance significantly their efficiency.

To measure the effectiveness of a catalytic system, several magnitudes are used.

The photochemical quantum yield, ϕ, measures the rate between irradiation and the amount of product obtained. This can refer to absorbed photons, (internal quantum yield, ϕ_I) or incident photons (apparent quantum performance, ϕ_A)

$$\varnothing_I = \frac{[\text{Product}] \times \text{n. of } e^-}{[\text{Absorbed photons}]} \times 100$$
$$\varnothing_A = \frac{[\text{Product}] \times \text{n. of } e^-}{[\text{Incident photons}]} \times 100 \quad (1)$$

The turnover number (TON) is the number of cycles a catalyst performs during its lifetime. That is, it is the molar ratio between CO_2 reduction products and catalyst

$$\text{TON} = \frac{[\text{Product}]}{[\text{Catalyst}]} \quad (2)$$

The turnover frequency (TOF) measures the number of catalytic cycles per unit of time, indicating the speed of the reaction

$$\mathrm{TOF} = \frac{\mathrm{TON}}{\mathrm{Reaction\ time}} \tag{3}$$

Finally, the selectivity can be quantified as the percentage molar ratio between the target product and the total amount of products

$$\mathrm{Selectivity} = \frac{\left[\mathrm{Target\ product}\right]}{\left[\mathrm{Total\ products}\right]} \times 100 \tag{4}$$

In the following, some of these magnitudes will be used to compare the efficiency of the catalytic systems analyzed.

3. Polypyridyl Ligands-Based Systems

The first examples of molecular catalytic systems for the selective photoreduction of CO_2 to CO were developed by Lehn's group in the early 1980s.[64] They used Re(I) bipyridine carbonyl complex *fac*-[Re(Bpy)(CO)$_3$(X)] (**ReBpy**, Bpy = 2,2′-bipyridine; X = Cl, Br, **Scheme 2**), which acted as photosensitizer and catalyst, and triethanolamine (TEOA) as electron donor, in dimethylformamide (DMF) as solvent.[64,65] The photochemical process took place under visible-light irradiation and produced CO with a quantum yield of 14% and a Faradaic efficiency of 98% (entry 1, **Table 2**). The catalytic mechanism proposed is represented in Scheme 2.

These Re complexes have the advantage that they act both as catalysts and photosensitizers, but they showed poor photostability due to decomposition processes that formed bimetallic species, what truncated the absorption in the visible region.[66] To overcome these problems, the reaction was conducted with an excess of halide[64] or increasing the CO_2 pressure.[67] Due to the efficiency of this Re(I) carbonyl-based system that does not need a photosensitizer, it has been anchored in different supports.

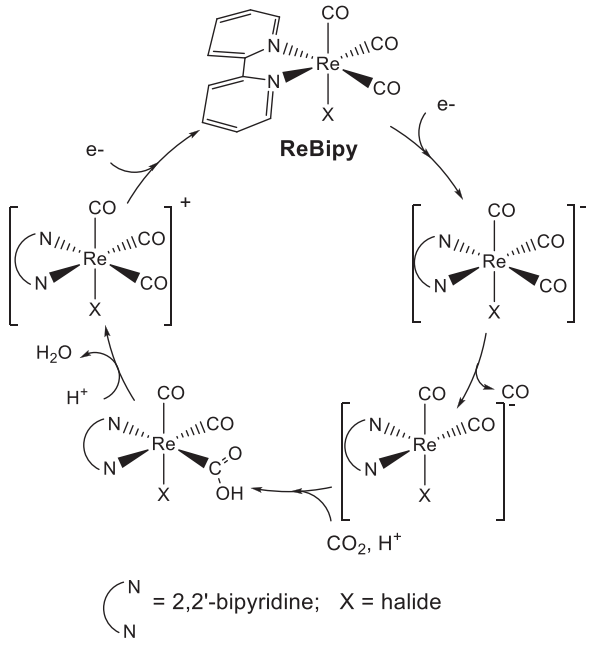

Scheme 2. A proposed possible mechanism for the re-catalyzed reduction of CO_2 to CO. Adapted with permission.[64,65] Copyright 1983, RSC, Copyright 1986, John Wiley and Sons.

Immobilization of ReBpy on mesoporous silica (ReBpyCONH@SiO_2, **Figure 1**) through a covalent attachment resulted in a material with higher photostability and activity than the molecular complex and the physically silica adsorbed complex.[59,68] The complex was attached covalently through an amido function generated by modification of the silica surface with 3-aminopropyltrimethoxysilane and reaction with 4,4′-bis(chlorocarbonyl)-2,2′-bipyridine followed by coordination of the Re precursor. The diamide material obtained had an extended conjugation which caused a redshift in the metal to ligand charge transfer band (MLCT) from 369 to 396 nm in the visible range, advantageous for absorbing the sunlight. With the optimized synthesis of the supported material, the TON obtained in the production of CO reached a value of 6.9 mol CO converted/mol Re in 4 h (entry 2, Table 2), and it increased twofold in the presence of $[Ru(Bpy)_3]^{2+}$ (**RuBpy**) as photosensitizer (entry 3, Table 2).[68] The presence of the electron-withdrawing amide groups decreased the photocatalytic activity of the Re(I) bipyridine-derived catalysts (entries 2 and 3 vs 4, Table 2), but in the presence of RuBpy as a PS, higher activity was observed. The authors proposed that the amide groups favored the intermolecular electron transfer between the photoexcited PS, $[Ru(Bpy)_3]^{\bullet+}$, and the Re(I) catalyst.[68]

A strategy to increase the catalytic activity is to tether the molecular catalysts in photoactive supports such as modified with chromophores mesoporous silica[69] or TiO_2.[73] Thus, the Re(I) bipyridyl fragment was anchored in the channels of a periodic mesoporous organosilica (PMO) as reported by Takeda et al. The PMO contained biphenyl chromophores in the framework (**ReBpy@PMO**, Figure 1), which act as light-harvesting antennas with good energy transfer to the Re(I) fragment.[69] Fluorescence experiments at 260 nm showed that the isolated PMO material had a strong emission at λ_{max} 380 nm attributed to the biphenyl groups, while irradiation of **ReBpy@PMO** at the same wavelength produced a new emission band at the 450–700 nm region assigned to the Re complex. This suggested that the excitation energy absorbed by the biphenyl groups is fully transferred to the Re complex. Photocatalytic experiments were performed illuminating **ReBpy@PMO** at the biphenyl excitation range (λ = 280 nm) in a CO_2 saturated solution of CH_3CN/TEOA (5/1 v/v). The system produced CO at an apparent quantum yield $\Phi_{A,CO}$ of 1.2% during the initial 5 h to reach a TON of 2.2 after 24 h (entry 5, Table 2). The irradiation of the catalytic system at 365 nm, the range of excitation of the Re complex, produced a smaller evolution of CO (4.4-fold less). This confirmed that the biphenyl group increases the photoactivity of the Re catalyst. Furthermore, photoexperiments in the absence of CO_2 compared with the molecular complex revealed that the PMO support leads to a more stable material decreasing the deactivation time.

In a similar approach, Liu and co-workers used benzene-bridged functionalized nanotubes containing bipyridine groups to anchor a Re(CO)$_3$Cl fragment (**ReBpy@PMONT**, Figure 1).[70]

Table 2. Results of CO_2 photoreduction obtained with pyridyl based supported catalyst.

Entry[a)]	Catalyst@support	Conditions: PS/SD/solvent/ λ nm/ t [h]	Main product (TON)[b)]	Selectivity %, (product)	Ref.
1	**ReBpy**/NEt_4Cl	-/TEOA/DMF (1:5 v/v)/250 W Xe λ >400 nm/4 h	CO (48)	100 (CO)	[64,65]
2	**ReBpyCONH@SiO_2**	-/TEOA/DMF (1:3 v/v)/Xe/4 h	CO (6.9)	n.i.	[68]
3	**ReBpyCONH@SiO_2**	**RuBpy**/TEOA/DMF (1:3 v/v)/Xe λ >475 nm/4 h	CO (11)	n.i.	[68]
4	**ReBpy**	-/TEOA/DMF (1:3 v/v)/ Xe/4 h	CO (30)	n.i.	[68]
5	**ReBpy@PMO**	-/TEOA/CH_3CN (1:5 v/v)/300 W Xe λ = 280, 365 nm/24 h	CO (2.2)	n.i.	[69]
6	**ReBpy@PMONT**	-/TEOA/H_2O/CH_3CN (1:8:7 v/v)/λ > 420 nm/8 h	CO (19.30) H_2 (1.23)	94 (CO)	[70]
7	**Re@BPy-PMO**	-/BIH/TEOA/CH_3CN (1:5 v/v)/12 mW Xe λ = 400 nm/24 h	CO (5.6)	n.i.	[71]
8	**Re@BPy-PMO**	**RuBpy**/BIH/TEOA/DMF (1:5 v/v)/12 mW Xe λ = 400 nm/24 h	CO (30.1) H_2 (1.7)	95 (CO)	[71]
9	**Re@BPy-PMONT**	**RuBpy**/BIH/TEOA/DMF (1:5 v/v)/2 mW λ = 450 nm/24 h	CO (30.4)	n.i.	[72]
10	**ReBpyPO$(OH)_2$@TiO_2**	-/TEOA/DMF (1:3 v/v)/λ > 400 nm/ 24 h	CO (62)	n.i.	[73]
11	**RePyBn-rGO@TiO_2**	-/TEOA/DMF (1:9 v/v)/300 W Xe/12 h	CO (151.92)[c)] (TOF 12.66 h^{-1})	100 (CO)	[74]
12	**RePyBn**	-/TEOA/DMF (1:9 v/v)/300 W Xe/12 h	CO (25.92)[c)] (TOF 2.16 h^{-1})	100 (CO)	[74]
13	**ReBpy-4-COOH@NbNS**	-/TEOA/DMF (1:5 v/v)/300 W Xe λ >400 nm/20 h	CO (58) (TOF 2.9 h^{-1})	100 (CO)[d)]	[75]
14	**ReBpy@ZrP**	**RhB**/TEOA (1:4 v/v /Xe λ > 400 nm/1 h	CO (9)	n.i.	[76]
15	**ReBpy-5-COOH@UiO-67**	-/TEA/CH_3CN (1:20 v/v)/450 W Xe λ >300 nm/6 h	CO (5, 10.9 at 20 h) H_2 (0.5, 2.5 at 20 h)	91 (CO, 81, 20 h) 9 (H_2)	[77]
16	**ReBpy@PyPOP**	-/TEA/CH_3CN (1:9)/150 W Hg λ >300 nm/20 h	CO (5) H_2 (8.8)	36 (CO) 64 (H_2)	[66]
17	**ReBpy@CPOP**	-/TEA/CH_3CN (1:9 v/v)/300 W Xe λ >390 nm/4 h	CO (1.9)[e)] H_2 (0.04)[e)]	97.8 (CO) 2.2 (H_2)	[78]
18	**ReBpy@CTF1**	-/TEOA/CH_3CN (1:4 v/v)/300 W Xe λ = 200–1100 nm/10 h	CO (4.8)[c)] CH_4 (0.19)[c)]	96 (CO) 4 (CH_4)	[79]
19	**ReBpy@CTF2**	-/TEOA/CH_3CN (1:15 v/v)/225 W Xe λ = 420 nm/20 h	CO (48)	98 (CO) 2 (H_2)	[80]
20	**RuBpyBim@GO**	-/H_2O/DMF (1:4 v/v)/20 W White LED/24 h	MeOH (4)[f)]	100 (MeOH)	[81]
21	**RuBpy$CH_2PO_3H_2$@C_3N_4**	-/TEOA/CH_3CN (1:4 v/v)/450 W Xe λ > 400 nm/5 h	HCO_2H (>200)	82 (HCO_2H) 12 (CO) 5 (H_2)	[82]
22	**$RuCl_2(CO)_2$@MOF-253**	-/TEOA/CH_3CN (1:10 v/v)/Xe λ = 420–800 nm/8 h	CO (7.1) $HCOO^-$ (2.9) H_2 (0.4)	68 (CO) 28 ($HCOO^-$) 4 (H_2)	[83]
23	**RuRe@PMO-Acd**	-/BIH/TEOA/DMF (1:5 v/v)/500 W Hg λ = 405 nm/24 h	CO (635) H_2 (10)	98 (CO)	[84]
24	**RuRu′@Bpy-PMO**	-/BNAH/DMA/H_2O (9:1 v/v)/500 W Hg λ > 430 nm/1 h	CO (95) $HCOO^-$ (67) H_2 (17)	53 (CO) 37.5 ($HCOO^-$) 9.5 (H_2)	[85]
25	**RuRu′@Ag-TaON**	-/CH_3OH/500 W Hg λ > 400 nm/9 h	CO (2.8) HCOOH (41) H_2 (28)[h)] HCOH (64)[g)]	99 (HCOOH)[h)]	[86]

Table 2. Continued.

Entry[a)]	Catalyst@support	Conditions: PS/SD/solvent/ λ nm/ t [h]	Main product (TON)[b)]	Selectivity %, (product)	Ref.
26	**RuRu′@Ag-TbTaON**	-/TEOA/CH_3CN (1:4 v/v)/400 W Hg $\lambda > 400$ nm/15 h	HCOOH (18)	n.i.	[87]
27	**RuRu′@Ag-C_3N_4**	-/TEOA/DMA (1:4 v/v)/400 W Hg $\lambda > 400$ nm/5 h	HCO_2H (3110) HCO_2H (>33 000, 48 h)	99 (HCO_2H)	[50]
28	**PdBpy@SiO_2Rf**	-/TEA/DMF (1:5 v/v)/500 W Hg $\lambda > 360$–440 nm/18 h, 4 Mpa, 373 K	CO (1184.4)[h)] H_2 (9)[i)]	>99 (CO)[j)]	[88]
29	**NiTpySH@CdS**	-/TEOA/H_2O pH = 6.7/Solar simulator $\lambda > 400$ nm/18 h	CO (20)	>90 (CO)	[89]
30	**NiTpy@$CsPbBr_3$**	-/Etyl acetate/H_2O (49/1 v/v)/ 300 W Xe $\lambda > 400$ nm/1 h	CO (1252 μmol g^{-1}) CH_4	≈90 (CO) ≈10 (CO)	[90]
31	**CoTpyP@TiO_2**	-/Cellobiose/CH_3CN/$NaOAc_{aq}$ (3:1 v/v)/solar simulator/24 h	$HCOO^-$ (103) CO (92) H_2 (72)	38 ($HCOO^-$)	[91]
32	**CoQpy@C_3N_4**	-/BIH/CH_3CN/100 W Xe $\lambda > 400$ nm/24 h	CO (128) H_2 (6.6)[c)]	98 (CO)	[92]
33	**Mn@Bpy-PMO**	**RuBpy**/BIH/TEOA/CH_3CN (1/5 v/v)/300 W Xe $\lambda > 400$ nm/5 h	$HCOO^-$ (292) CO (168) H_2 (72)	55 ($HCOO^-$)	[93]
34	**Mn@UiO-67**	**RuBpyMe**/TEOA/DMF (1:4 v/v)/LED $\lambda = 470$ nm/18 h	$HCOO^-$ (110) CO (4.5) H_2 (1)	96 ($HCOO^-$)	[63]

[a)]PS = Photosensitizer, SD = sacrificial electron donor, n.i. = not indicated, TEA = triethylamine, TEOA = triethanolamine, DMF = dimethylformamide, BIH = 1,3-dimethyl-2-phenyl-2,3-dihydro-1*H*-benzoimidazole, BNAH = 1-benzyl-1,4-dihydronicotinamide, DMA = *N*,*N*-dimethylacetamide, **RhB** = Rhodamine B; [b)]TON = Turnover number ($mol_{product}/mol_{catalyst}$), TOF = turnover frequency ($mol_{CO}/mol_{catalyst}h$); [c)]Estimated from TOF reported values; [d)]Only gaseous products analyzed; [e)]Estimated from Re content 0.88 mmol g^{-1}[78]; [f)]Estimated from Ru content 0.51 mmol g^{-1}; [g)]Estimated from other TON data; [h)]Estimated from TOF 65.8 h^{-1}; [i)]Estimated from TOF 0.5; [j)]Including H_2.

The fit of the bipyridine contents to the framework allowed to obtain a material with high diffusion of the reactants and absorption of CO_2. To decrease the competitive hydrogen generation, the surface silanol groups were transformed to trimethylsilyl groups to decrease the hydrophobicity and the tolerance to water. The catalytic system consisting of **ReBpy@PMONT** with TEOA in a solution of H_2O/CH_3CN (1.14:1 v/v) was active in the photoreduction of CO_2 to CO (TON 19.30 after 8 h, entry 6, Table 2) with high selectivity on CO (94%). The stability of the supported Re bipyridine system increased in the PMO material allowing to maintain the catalytic activity after five cycles (total TON 134 after 40 h) while the molecular system was deactivated under the same conditions after two cycles.[70] The reported apparent quantum yield reached 0.146%.

Alternatively, the bipyridyl groups were incorporated as the organic component of organosilica materials to immobilize the rhenium complex by coordination. Thus, rhenium carbonyl was supported on a bipyridine-periodic mesoporous organosilica (**Re@Bpy-PMO**, Figure 1)[71] and bipyridine-modified organosilica nanotubes (**Re@Bpy-PMONT**, Figure 1).[72]

The activity of the **Re@Bpy-PMO** in the photoreduction of CO_2 was modest but it increased 5.4-fold times in the presence of 1,3-dimethyl-2-phenyl-2,3-dihydro-1*H*-benzoimidazole (BIH) as electron donor and when the **RuBpy** photosensitizer was also introduced in the Bpy-PMO support (entries 7 and 8, Table 2).[71] The apparent quantum yield, in this case, increased from 0.4% (entry 7, Table 2) to 2.2% (entry 8, Table 2). Unfortunately, the activity of this catalytic system largely decreased when it was reused in a second run. Higher efficiency in the light absorption was obtained with the similar system prepared using tubular organosilica nanotubes with large pore sizes (**Re@Bpy-PMONT**, Figure 1), achieving a quantum yield up to 15.1% in the presence of **RuBpy** as PS (entry 9, Table 2).[72] An enhancement of the catalytic activity was observed supporting the Re bipyridyl fragment on TiO_2. The bipyridyl ligand was modified by the introduction of phosphonic groups (**ReBpyPO(OH)$_2$**, **Scheme 3**) to increase the interaction with the surface of the TiO_2 nanoparticles.[73] The complex was immobilized in the solid by impregnation in an aqueous solution. Characterization by Fourier transform infrared (FTIR) and X-ray photoelectron spectroscopy (XPS) confirmed the formation of the **ReBpyPO(OH)$_2$@**TiO_2 material. The supported material increased the photocatalytic activity of the molecular system **ReBpyPO(OH)$_2$** up to 26-fold times, achieving a TON of up to 62 at 24 h irradiation (TOF 8 h^{-1} at 3 h, entry 10, Table 2). The detection of intermediate lifetimes and the measurement of the energy of the photogenerated excited states by time correlated-single photon counting and transient absorption spectroscopy techniques allowed to propose a catalytic cycle for the **ReBpyPO(OH)$_2$@TiO$_2$** which is similar to the one proposed for the homogenous system (Scheme 3). A reduced species is formed [**ReBpyPO(OH)$_2$**]$^-$, which lifetime is longer in the supported complex than in the homogenous solution. The authors attributed the higher stability of the reduced intermediate to the

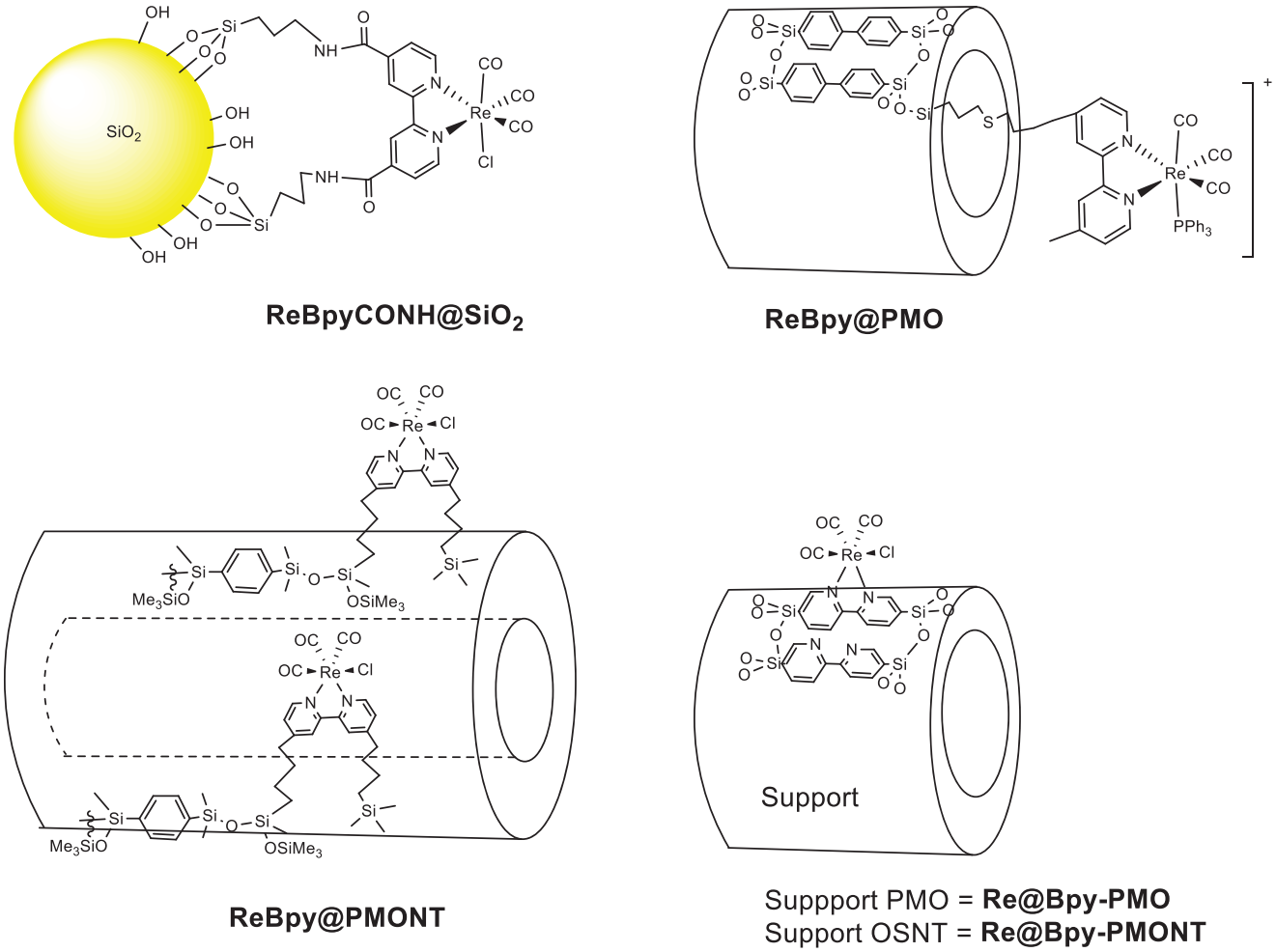

Figure 1. Immobilization of ReBpy in mesoporous silica (ReBpyCONH@SiO_2) (adapted with permission.[59] Copyright 2012, Elsevier) and periodic mesoporous organosilica (ReBpy@PMO) (adapted with permission.[69] Copyright 2010, American Chemical Society), ReBpy@PMONT (adapted with permission.[70] Copyright 2019, Elsevier), Re@Bpy-PMO (adapted with permission.[71] Copyright 2016, John Wiley and Sons) and Re@Bpy-PMONT.[72]

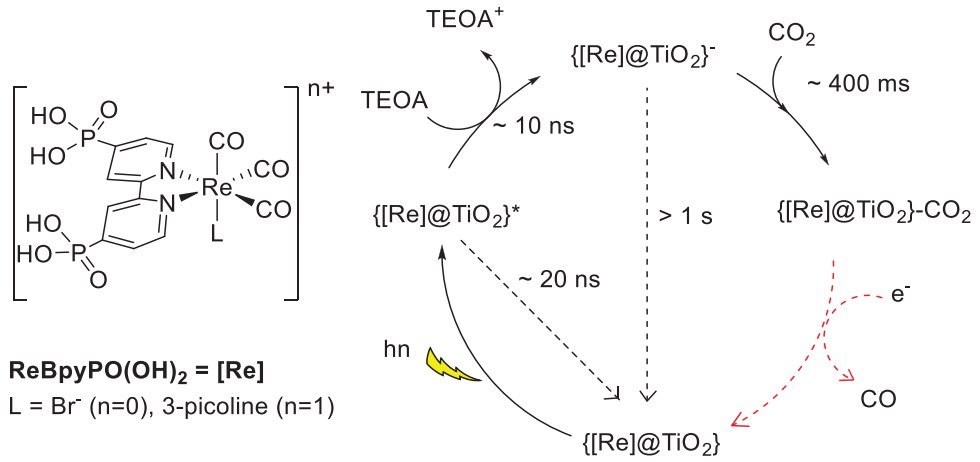

Scheme 3. Proposed catalytic mechanism for **ReBpyPO(OH)$_2$**@TiO_2 photocatalyzed reduction of CO_2 to CO under visible light. Lifetimes ($t_{50\%}$) of some species are included. The dotted lines represent the deactivation paths. The second reduction (dotted red lines) was not observed. Adapted with permission.[73] Copyright 2015, John Wiley and Sons.

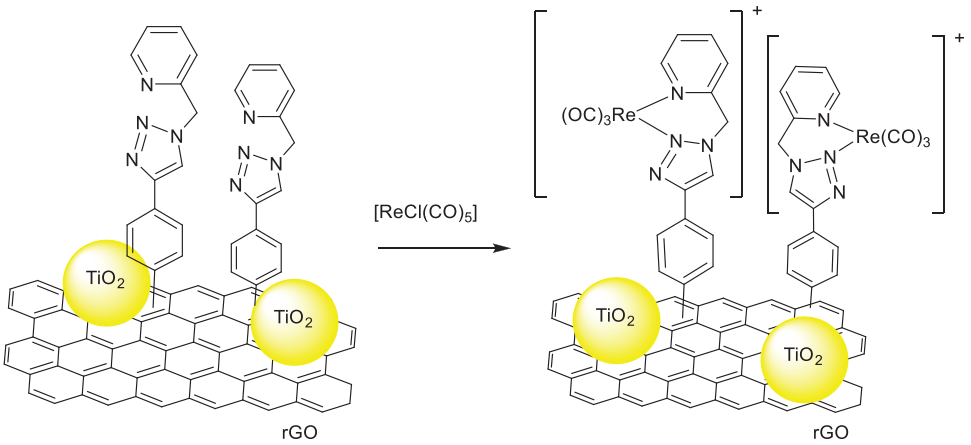

Scheme 4. Preparation of the **RePyBn**-rGO@TiO_2 composite. Adapted with permission.[74] Copyright 2016, John Wiley and Sons.

scaffolding provided by the support, what resulted in a higher activity of the immobilized system. Furthermore, the supported material decreased the formation of inactive dimeric Re species. The studies also concluded that the second reduction necessary for CO_2 to CO occurred through the sacrificial electron donor TEOA.

To improve the electron transfer processes of the photocatalytic reduction of CO_2, graphene oxide (GO) was also used as support. Graphene and derivatives can act as efficient electron storage materials[94] to improve the catalytic performance of photocatalysts. The synthetic strategy included a modification of reduced GO (rGO) with a triazole derivative to covalently graft the Re(I) carbonyl derivative, and further combined it with TiO_2 to form the **RePyBn-rGO@TiO_2** composite (**PyBn** = 1-(2-picolyl)-4-phenyl-1*H*-1,2,3-triazole, **Scheme 4**).[74] The presence of the complex in the support was confirmed by IR and XPS and transmission electron microscopy confirmed the presence of the graphene sheets containing the spherical nanoparticles of TiO_2. A significant enhancement of the catalytic activity was achieved in the visible light photocatalytic reduction of CO_2 by **RePyBn-rGO@TiO_2** composite in DMF with TEOA producing only CO as a reduction product with TOF up to 12.66 h^{-1} after 12 h irradiation (entry 11, Table 2). The support of the Re complex in the composite increased the catalytic activity sixfold with respect to the molecular homogenous system under the same conditions (entry 12, Table 2). Furthermore, the stability also improved since the catalyst was separated from the solvent and kept its activity in five cycles of 12 h each. The mechanism of the reaction was analyzed by time-resolved infrared spectroscopy. Two species, attributed to the reduced catalytic material, [$Re^{II}PyBn^{\bullet-}$-rGO-DMF]$^+$@TiO_2, and a CO_2 adduct, [$Re^{II}PyBn^{\bullet-}$-rGO-CO_2-TEOA]$^+$@TiO_2 with lifetimes of hundreds of microseconds were detected together with the formation of CO absorbed in the material. Control experiment with only the rGO without the TiO_2 revealed that this material is involved in the electron storage and transfer. Based on these observations, a mechanism was proposed (**Scheme 5**) in which the process initiates with the excitation of one electron in the photoactive TiO_2/rGO material. This electron is transferred to reduce the complex to the rhenium(I) species and, by a metal to ligand charge transfer process it is finally transferred to the **PyBn** ligand by quenching with TEOA. The chloride ligand is then replaced by the solvent DMF and there are electron transfer processes between the ligand and the rGO. It is proposed that TEOA is involved both in the CO_2 activation step and as a H^+ donor to produce CO.

Other inorganic solids such as niobates[75] and phosphates[76] were used as supports giving high selective photoreduction of CO_2-to-CO but modest TONs. Thus, a Re(I) bipyridine complex modified with carboxylate groups, **ReBpy-4-COOH** (**Figure 2**), was supported onto the surface of hexaniobate nanoscrolls (**NbNS**) to improve the stability of the rhenium catalyst **ReBpy-4-COOH@NbNS**.[75] The adsorption of the complexes in the **NbNS** produced a red-shift of the MLCT bands absorption spectra. The photoreduction of CO_2 in absence of PS in DMF using TEOA produced CO with a 20% higher TON (TON 58) than with TiO_2 and sixfold larger than the value obtained with the molecular system **ReBpy-4-COOH** under the same conditions after 20 h of irradiation (entry 13, Table 2). Respect to the phosphate support, the Re-bipyridine fragment was intercalated in the layered structure of zirconium phosphate $Zr(HPO_4)_2 \cdot H_2O$ by ion exchange or phase boundary mechanism (**ReBpy@ZrP**).[76] The photocatalytic activity of this material was enhanced 3.7-fold times by the addition of an organic dye such as Rhodamine B (**RhB**) achieving a TON up to 9 after 1 h (entry 14, Table 2). The **ReBpy@ZrP** was active for three cycles although **RhB** had to be replaced each run.

The **ReBpy** fragment has been also introduced in MOF structures[77] to combine its capacity of harvesting light and act as photocatalysts.[95] The zirconium-based $Zr_6O_4(OH)_4$(**Bpy-5-COOH**)$_6$ (UiO-67, **Bpy-5-COOH** = 2,2′-bipyridine-5,5′-dicarboxylic acid) MOF was doped with the **ReBpy-5-COOH** complex (Figure 2) to form **ReBpy-5-COOH@UiO-67**. The [$Zr_6(\mu_3\text{-}O)_4(\mu_3\text{-}OH)_4$(**Bpy-5-COOH**)$_6$] material was prepared by treating $ZrCl_4$ with a combination of **Bpy-5-COOH** and **ReBpy-5-COOH** in DMF at 100 °C. Photocatalytic activity of **ReBpy-5-COOH@UiO-67** in the CO_2 reduction in acetonitrile, using triethylamine (TEA) as a sacrificial reducing agent produced CO with a TON of 5 mols per catalytic site with a 91% selectivity respect to H_2 in 6 h (entry 15, Table 2). The catalytic system was separated by centrifugation and used again and was active in two catalytic cycles but became inactive in the third run due

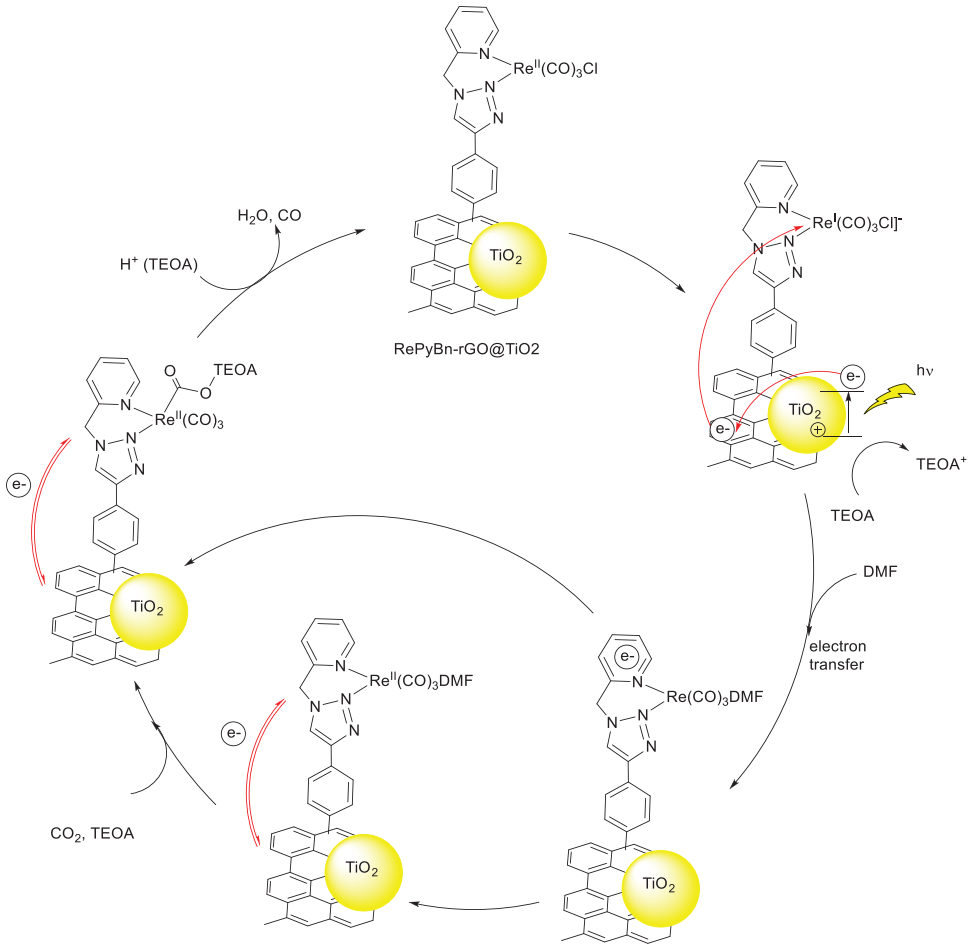

Scheme 5. Mechanism proposed for the CO_2-to-CO photoreduction catalyzed by **RePyBn**-rGO@TiO_2 composite. Reproduced with permission.[74] Copyright 2016, John Wiley and Sons.

to rhenium leaching from the MOF structure (43.6%). Nevertheless, the activity obtained with the homogenous **ReBpy** systems was lower, what indicates that the stability of the system increased due to the MOF structure.[77]

Another family of supports largely used are porous organic polymers (POPs) which have high surface areas and contain functionalities such as polypyridinic,[66] polymeric carbazol-based structures,[78] and covalent triazine frameworks,[79,80] able to coordinate metal fragments, what also lead to an increase in the CO_2 absorption ability of the support. The Re(I) bipyridyl containing catalytic materials based on this kind of supports produced, in most cases, selectively CO without the presence of a photosensitizer but the TON did not exceed the values reported for the molecular **ReBpy** system. In the case of the **ReBpy** fragment incorporated in the pyridyl POP (**ReBpy@PyPOP**, **Figure 3**), this material photocatalyzed the CO_2 to CO reduction with the formation of H_2 (H_2/CO = 1.4–2.2) in a CH_3CN/TEA reaction medium under light irradiation at λ 300–550 nm. The rate of CO generation (d[CO]/dt = 4.6 ± 0.5 μmol min^{-1} mmol Re^{-1} over t = 110–1200 min), although was lower than the one produced by the molecular species **ReBpy**, was more stable over time than with the molecular catalyst and reached a TON_{CO} = 5 after 20 h and a TON_{H2} = 8.8 (entry 16, Table 2). The higher stability of the **ReBpy@PyPOP** material was attributed to the fact that the porous structure prevented the interaction between rhenium centers avoiding the formation of inactive dimeric species.[66] In another case, reported by Liang et al., the rhenium fragment was incorporated in a polycarbazol POP (**ReBpy@CPOP**, Figure 3). This material showed uptakes of CO_2 in the range of 7.6–9.4 wt% at 273 K/1 atm.[78] The integration of the carbazole moieties in the framework induced a significant bathochromic shift of the absorption bands which increases the visible-light absorption ability. The generation of CO under visible light excitation in the presence of TEOA reached a rate of CO evolution up to 623 μmol g^{-1} h^{-1}

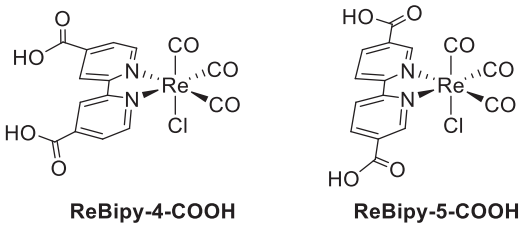

Figure 2. **ReBpy-4-COOH** and **ReBpy-5-COOH** incorporated in niobate nanoscrolls[75] and MOF UiO-67,[77] respectively.

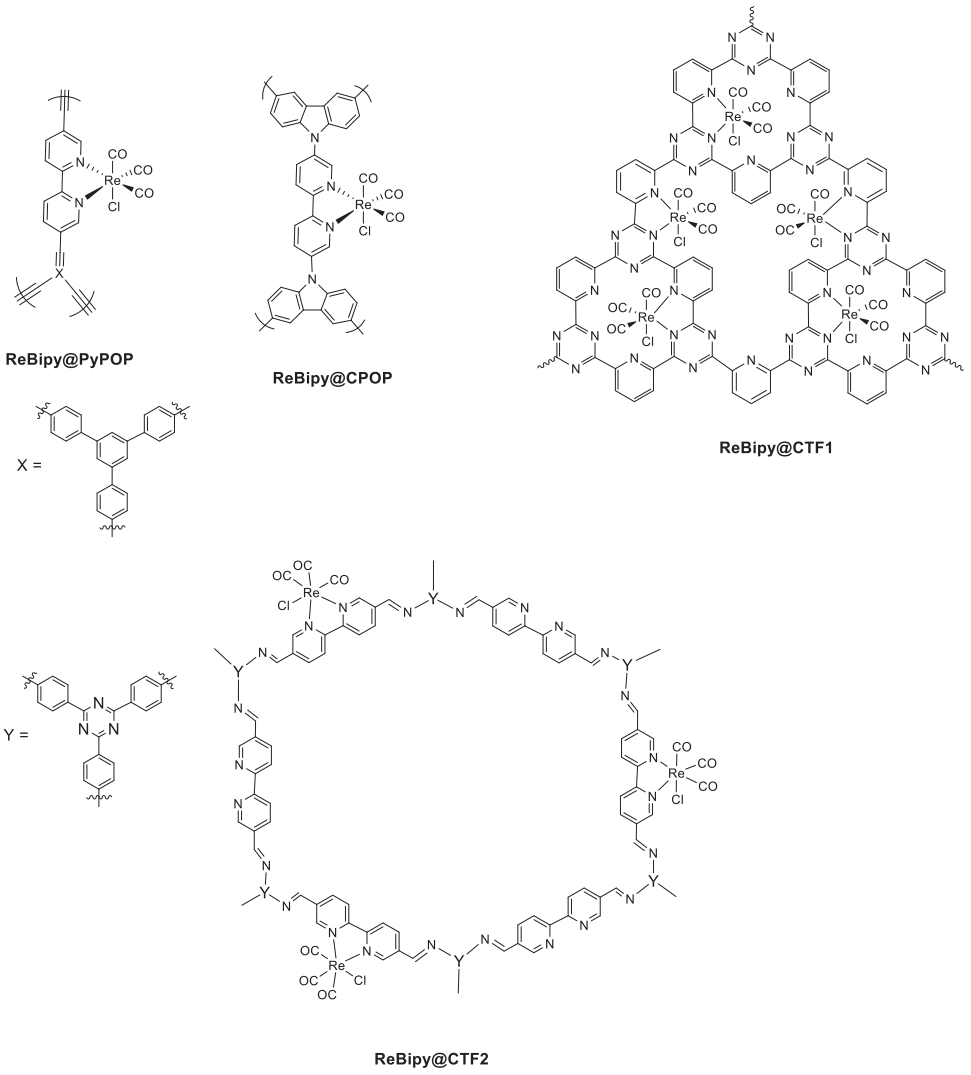

Figure 3. ReBpy fragment incorporated in POP (adapted with permission.[66,78] Copyright 2015, John Wiley and Sons and 2019, American Chemical Society) and covalent triazine frameworks (CTF) (adapted with permission.[79] Copyright 2018, Royal Society of Chemistry). Proposed structure for ReBpy@CTF2 (adapted with permission.[80] Copyright 2018, American Chemical Society).

with a higher selectivity in the CO (97.8%) (entry 17, Table 2). The catalytic material was reused in four consecutive 10 h cycles, keeping ≈83% of the initial activity. Finally, the Re bipyridine fragment was incorporated in two different covalent triazine frameworks (CTFs).[79] In the first case, **ReBpy@CTF1** (Figure 3)[79] produced CO photocatalytically with a TON of 4.8; the CO evolution rate within 10 h (entry 18, Table 2) under full light irradiation (λ = 200–1100 nm) in a solid-gas system was 353.05 μmol g^{-1} h^{-1}, which performed better than the liquid–gas system. In the second case, a similar approach was reported by Yang et al. who constructed a photoactive covalent organic framework using as building block 4,4′,4″-(1,3,5-triazine-2,4,6-triyl) trianiline and 2,2-bipyridyl-5,5- dialdehyde in which Re was attached through coordination to the bipyridyl fragments (**ReBpy@CTF2**, Figure 3).[80] The incorporation of the Re fragment in the triazine framework produced a broadening and increased lifetime of the intramolecular charge transfer band (ICT) suggesting that the charge recombination is inhibited by the presence of the Re complex. The catalytic system consisting of **ReBpy@CTF2** in the presence of TEOA produced selectively CO (98%) with a higher TON (48, t > 20 h) than in the case of **ReBpy@CTF1** (entry 18 vs 19, Table 2) and remarkably 22 times better than the molecular system under the same conditions according to the authors. The catalytic activity was maintained for at least three cycles. An induction period was necessary for the activation of the material that was attributed to the formation of the exited ICT state. Mechanistic studies suggest that the photoexcitation of **ReBpy@CTF2** produces a reduction of the Re center.

It can be seen that in general, Lehn's Re bipyridyl-based photocatalysts have been immobilized on solids mostly through modification of the bipyridine skeleton to favor the interaction with the support or the reaction of functional groups of the support surface has been induced to covalently bond the metallic center. The immobilization of the Re(I) molecular species yielded materials with higher stability than the molecular

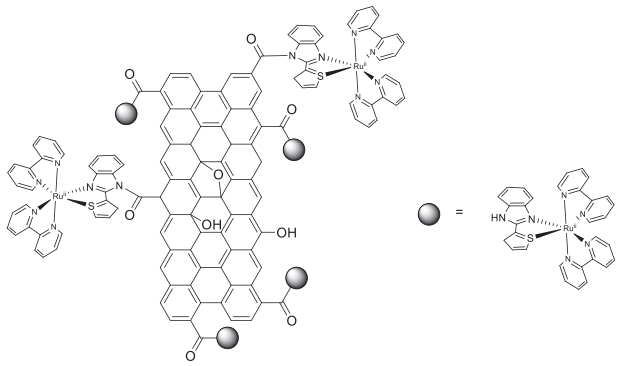

Figure 4. Ru(II) 2,2′-bipyridine complex 2-thiophenyl benzimidazole ligand (Bim) immobilized in modified GO (**RuBPyBim@GO**). Adapted with permission.[81] Copyright 2015, Royal Society of Chemistry.

catalyst. This allowed to obtain systems more active than the molecular complexes (TON ~ 10^2) while keeping the high selectivity in the CO_2 photoreduction to CO.

As we have discussed, **RuBpy** has been introduced in Re(I) systems as PS to increase the light-harvesting ability of the catalyst, but Ru bipyridine complexes were also reported to behave as catalysts for the CO_2 photoreduction.[96] In the case of ruthenium-based catalytic systems, the products of photoreduction are mainly MeOH and formic acid derivatives. A Ru(II) 2,2′-bipyridine complex containing a 2-thiophenyl benzimidazole ligand (**RuBPyBim@GO**, **Figure 4**) immobilized on graphene oxide through amide functionalization, produced MeOH in 2050 μmol g^{-1} of catalyst in 24 h irradiation without SD (estimated TON 4, apparent quantum yield 0.180%, entry 20, Table 2).[81] It was recycled with almost no loss of activity for three consecutive runs after separation by centrifugation.

The influence of the support was evidenced in another hybrid catalytic system obtained, from a phosphate-modified bipyridine Ru(II) complex adsorbed on the graphitic carbon nitride semiconductor with mesoporous structure mpg-C_3N_4 (**RuBpyCH$_2$PO$_3$H$_2$@C$_3$N$_4$**, **Figure 5**).[82] The graphitic carbide was responsible for light-harvesting and the Ru complex was the catalytic center for CO_2 photoreduction. In this case, formic acid was produced with an 82% selectivity and TON >200 in 5 h (entry 21, Table 2). CO and H_2 were also formed. Label experiments with $^{13}CO_2$ confirmed that CO_2 reduction was the origin of the HCO_2H formed and most of the CO formed.

As example of MOF as supports for Ru catalysts, **RuCl$_2$(CO)$_2$** species was introduced in the open N,N′-chelating sites of an aluminum-based MOF Al(OH)(**dcbpy**) (**dcbpy** = 2,2′-bipyridine-5,5′-dicarboxylic acid) MOF-253 (**RuCl$_2$(CO)$_2$**@MOF-253).[83] The material was prepared by refluxing the de-solvated MOF-253 in anhydrous methanol containing $[RuCl_2(CO)_3]_2$. X-ray diffraction (XRD), FTIR, and Fourier-transformed-extended X-ray absorption fine structure analysis confirmed the introduction of the species in the nonaltered MOF-253 structure, which preserved a high specific surface area (1085 m^2 g^{-1}). This material produced a mixture of CO, $HCOO^-$, and H_2 with TONs of 7.1, 2.9, and 0.4, respectively in 8 h (entry 22, Table 2). The incorporation of the $[Ru(\mathbf{Bpy})_2Cl_2]$ photosensitizer in the MOF-253-**RuCl$_2$(CO)$_2$** structure enhanced the formation of formate 12-fold while the CO production remained stable.

The importance of supporting also the PS was shown in a hybrid catalytic material for the photoreduction of CO_2 consisting of a solid PMO with acridone groups as light harvester and a heterodinuclear Ru-Re molecular catalyst was reported by Ueda et al. (**Figure 6**).[84] The combination of the PMO/acridone (PMO-Acd) with the binuclear complex increased the efficiency of the photoreduction of CO_2 to TON 635 and the selectivity in CO (>98%) (entry 23 vs entry 5, Table 2). The authors attributed this increase with respect to related PMO-supported materials to the ability of this system to absorb in the visible light region.[84]

In a different approach, the surface functionalization of bipyridine-modified PMO supports was used to immobilize two different ruthenium fragments, a $[Ru(Bpy)]_{2+}$ with PS functionality and a $RuCl_2(CO)_2$ one, which acts as a catalyst (**RuRu′@Bpy-PMO**, Figure 6).[85] The photochemical reduction of CO_2 (λ > 430 nm) with the **RuRu′@Bpy-PMO** was studied using 1-benzyl-1,4-dihydronicotinamide (BNAH) as the electron donor in a CO_2 saturated DMF/H_2O solution to produce a mixture of $CO/HCOO^-$ and H_2 reaching a total TON of 179 in 1 h (entry 24, Table 2). The TOF in the CO_2 reduction products $CO/HCOO^-$ was up to 162 h^{-1}. The catalytic activity was higher when the relative amount of Ru catalyst was higher and the selectivity

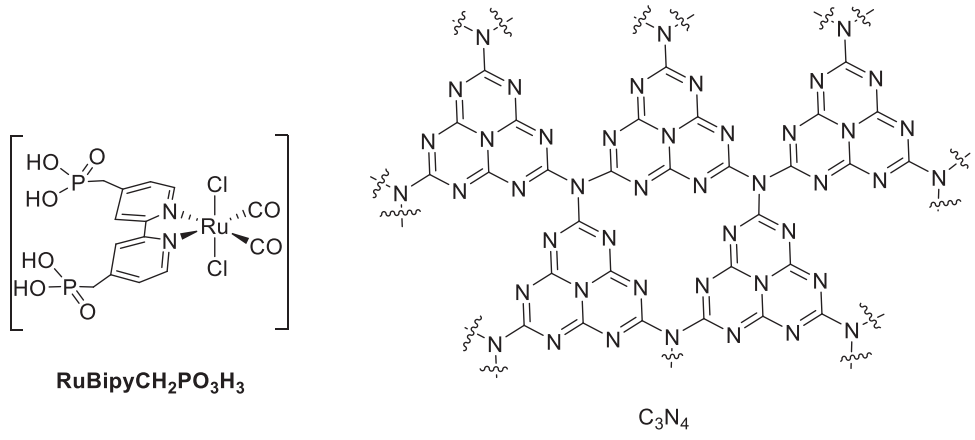

Figure 5. Structures of **RuBpyCH$_2$PO$_3$H$_2$** and graphitic mesoporous C_3N_4. Adapted with permission.[82] Copyright 2013, Royal Society of Chemistry.

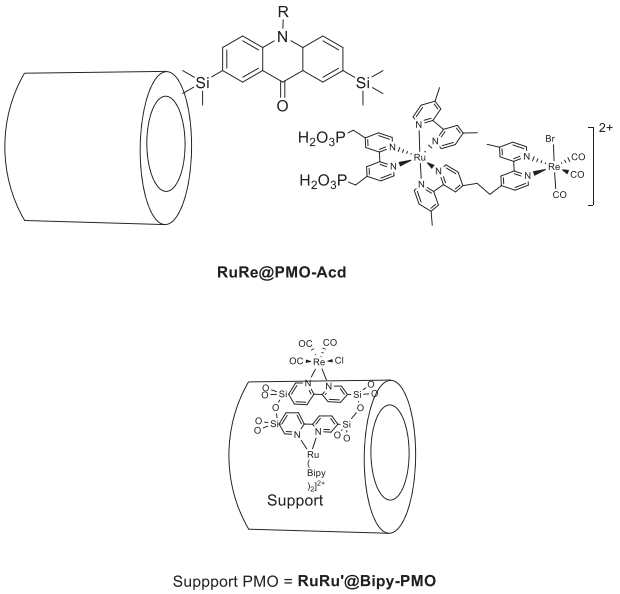

Figure 6. Structures of the components of **RuRe@PMO-Acd** (Acd = acridine) (adapted with permission.[84] Copyright 2014, John Wiley and Sons) and **RuRu'@Bpy-PMO** (adapted with permission.[85] Copyright 2017, John Wiley and Sons).

in CO was higher (53%) when the ratio Ru PS/Ru catalyst was higher. The system was recycled up to three cycles without loss of activity.[85]

The combination of a semiconductor and a molecular catalyst in which photosensitizer and catalyst are included in a bimetallic complex has shown high efficiency for CO_2 photoreduction. Sekizawa et al. reported a Ru(II) dinuclear complex that was adsorbed onto a semiconductor material consisting of a silver-loaded tantalum oxynitride (**RuRu'@Ag-TaON**, **Figure 7**).[86] A methanol CO_2 saturated dispersion of **RuRu'@Ag-TaON** produced a mixture of HCOOH, HCOH, H_2, and CO (TON_{HCOOH} = 41 after 9 h, entry 25, Table 2). Isotope-labeled experiments showed that CO was mainly (77%) obtained from the ruthenium carbonyl complex and formaldehyde came from methanol. A more modest activity toward the formation of formate was obtained with related ruthenium systems supported on defect fluorite-type Ln–Ta oxynitrides LnTaOxNy (**RuRu'@Ag-LnTaON**). The best TON reported was 18 obtained with the terbium material (**RuRu'@Ag-TbTaON**, entry 26, Table 2), although the selectivity was higher (99%) since acetonitrile was used as solvent instead of methanol.[87] The same RuRu' system supported on a graphitic carbon nitride with Ag nanoparticles (**RuRu'@Ag-C_3N_4**, Figure 7)[86] resulted in a higher active and selective photocatalytic material for the photoreduction of CO_2 to HCOOH.[50] With this catalytic system, Kuriki et al. reported a TON > 33 000 after 48 h (entry 27, Table 2) with selectivities in the range 86–99% even in aqueous solutions. The apparent quantum yield was lower (5.2%) than the reported for molecular mononuclear Ru complexes.[97]

The effect of increasing the CO_2 pressure in the photoreduction of CO_2 was studied in Pd-**Bpy** systems supported in CO_2-expanded liquids.[88] The bipyridine ligand was modified with perfluorinated chains to increase its affinity to fluorinated-modified silica used as support (**PdBpy@SiO_2Rf**, **Figure 8**). **PdBpy@SiO_2Rf** without PS was active in the photoreduction of CO_2 to CO achieving a TOF 65.8 h^{-1} at 4 Mpa and 373 K in the presence of TEA in the CO_2-expanded DMF medium (entry 28, Table 2). This value was six times larger than the one obtained with the unsupported system. The increase of activity was attributed to the higher stability of the system in the supported material.

To develop catalysts using abundant first-row transition metal-based systems, nickel[89,90] and cobalt complexes[91,92] were supported in different materials and used as catalysts for the photoreduction of CO_2. Thus, Reisner and co-workers developed a nickel terpyridine complex adsorbed onto the semiconductor CdS quantum dots that photocatalyzed the reduction of CO_2 to CO in aqueous media (**NiTpyR@CdS**; R = H, CO_2H, PO_3H_2, SH).[89] Thus, CO was obtained in high selectivity (>90%) under visible light irradiation (λ > 400 nm) in an aqueous system at pH 6.7 using the thiol derivative (**NiTpySH@CdS**) (entry 29, Table 2). The limit of stability of the system was estimated in 20 h reaching a TON of 20. The importance of the combination of molecular catalysts with semiconductors was proved with a similar Ni terpyridine-based system supported on halide perovskite nanocrystals ($CsPbBr_3$).[90] The hybrid material **NiTpy@$CsPbBr_3$** produced ≈26-fold higher yield (1252 µmol of CO/CH_4 g h, entry 30, Table 2) on the photoreduction of CO_2 to CO/CH_4 than when using the perovskite nanocrystals alone. The authors claimed that the Ni complex acted as specific catalytic site and electron sink to suppress the electron–hole recombination in the semiconductor perovskite material.

The sacrificial donor is often an expensive amine (TEOA) which forms a non-added value product. Lam and Reisner

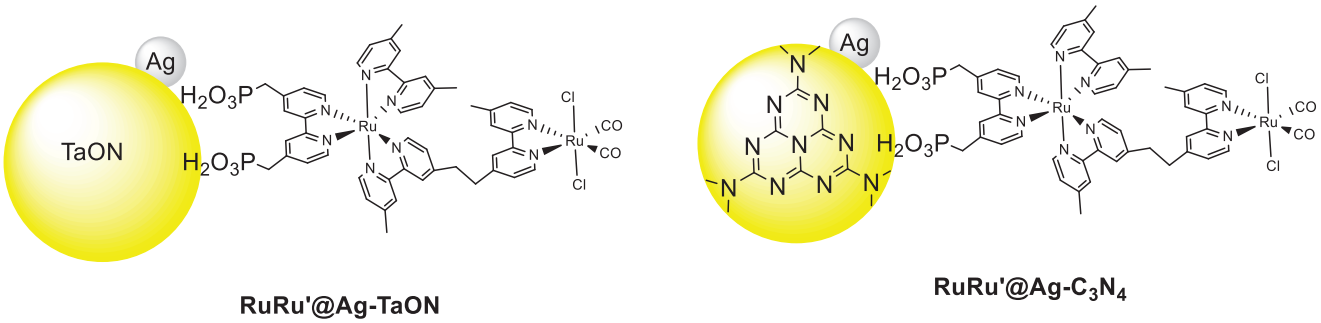

Figure 7. Structures of the components of **RuRu'@Ag-TaON**[86] and **RuRu'@Ag-C_3N_4**.[50]

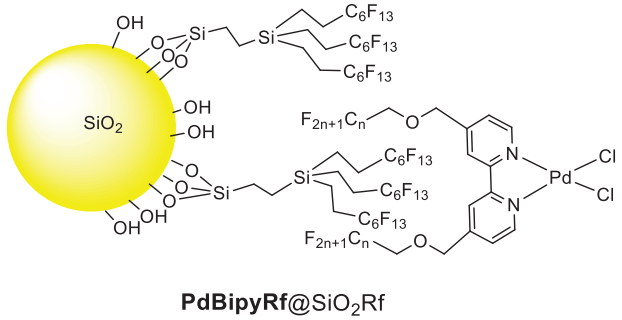

Figure 8. PdBpyRf catalyst supported onto fluorinated silica. Adapted with permission.[88] Copyright 2013, Elsevier.

proposed to use as a sacrificial donor a sustainable product whose oxidation produces a valuable product.[91] Thus, soluble biomass-derived oxygenates such as C_6 and C_5 sugars (glucose, galactose, and arabinose), disaccharides (maltose), and glycerol were used as SDs as models of this kind of compounds that yielded formate as an oxidation product. The molecular catalyst selected was a phosphonate-derived terpyridine cobalt(II) complex that was supported on a photoactive TiO_2 P25 anatase-rutile, **CoTpyP**@TiO_2 (**Scheme 6**). The catalyst was prepared in situ by self-assembling the two separated components. Using the biomass-derived soluble oxygenated substrates, the photoreduction of CO_2 with **CoTpyP**@TiO_2 produced mixtures of CO (up to 0.92 mmol g^{-1} TiO_2) and H_2 (up to 0.72 mmol g^{-1} TiO_2) in 24 h in a mixture CH_3CN:H_2O (entry 31, Table 2). Formate was also detected in the reaction. The ^{13}C label experiments concluded that formate was generated mostly by the oxidation of the oxygenated substrates. Polymeric biomass substrates such as cellulose could also be used as SD with an enzymatic pretreatment to fragment it into more soluble products. After a 24 h catalytic run, the photocatalyst was separated and redispersed in a pretreated cellulose dispersion saturated with CO_2. The recycled material kept 55% of the initial photoactivity.

A Co-quaterpyridine complex was covalently grafted on mesoporous graphitic carbon nitride C_3N_4 through amido linkages (**CoQpy@C_3N_4**, **Scheme 7**).[92] The hybrid material **CoQpy@C_3N_4** in the presence of BIH as SD and PhOH as proton donor under visible light irradiation ($\lambda > 400$ nm) produced selectively CO from CO_2 (selectivity 98%, entry 32, Table 2) at a modest TON of 128 after 24 h with remarkable stability in successive cycles in which fresh CO_2, BIH, and PhOH were added achieving a total TON of ≈500 cycles.

Other abundant first-row metal complexes, such as manganese, were supported on PMO or MOF structures and used in the photocatalytic reduction of CO_2. The already discussed strategy of using bipyridine-modified PMO materials to bond coordination compounds was used to immobilize [$Mn(CO)_5Br$] (**Mn@Bpy-PMO**, **Figure 9**).[93] This material in the presence of **RuBpy** and BIH/TEOA produced formate and CO as CO_2 reduction products with TON of 292 and 168, respectively (entry 33, Table 2). Recycling of the catalytic material provided a total TON of 484 and 239 for formate and CO, respectively, after three cycles although deactivation was observed after each cycle.

A Mn(I) carbonyl fragment was incorporated in a Zr(IV) MOF, UiO-67, using the bipyridine-5,5′-dicarboxylate linkers as coordination sites for Mn(I) (**Mn@UiO-67**, Figure 9).[63] This material in combination with [$Ru(BpyMe)_3$][PF_6]$_2$ (**RuBpyMe**, BpyMe = 4,4′-dimethyl-2,2′-bipyridine) as PS, BNAH as SD in a mixture of DMF/TEOA photocatalyzed the selective formation of formate (≈96%) with a TON of 110 after 18 h (entry 34, Table 2), higher than the one obtained with the separate components. The apparent quantum yield reached 6.74%. The authors proposed that the MOF structure inhibits the deactivation of the catalyst by dimerization and increases the stability of the reduced Mn species. The recycling experiments showed a decay of the activity of 66% after three 4 h cycles.

4. Cyclam Ligands-Based Systems

Complexes containing macrocyclic **cyclam** ligands (**cyclam** = 1,4,8,11-tetraazacyclotetradecane) have been often used in the photochemical CO_2 reduction.[98–100] The stability of the complexes under photochemical conditions and the catalyst recovery and recycling are the main challenges for these catalysts. Given the advantages provided by heterogenization, several studies have been focused on the use of heterogenized cyclam-based catalysis, in particular concerning Co and Ni complexes. When using silica and titania as supports, the formation of covalent bonds between the terminal hydroxyl groups on the surfaces is the most general strategy to graft the complexes.

[Co(**cyclam**)Cl_2]Cl has been used as the starting product for the preparation of the supported catalysts on TiO_2 and SiO_2.[101]

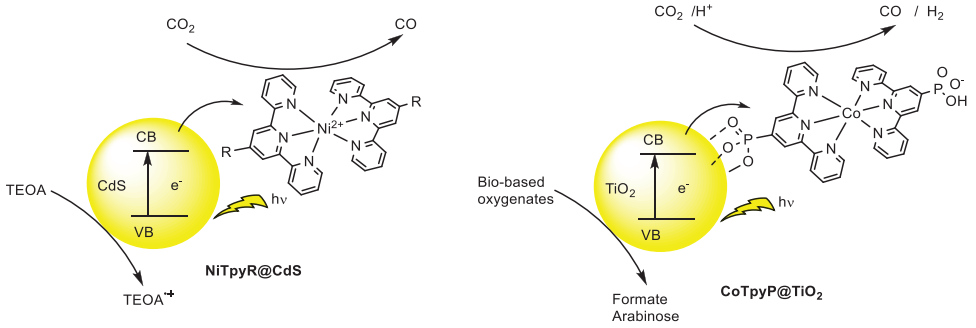

Scheme 6. Metal terpyridine-based systems supported on CdS (**NiTpy@CdS**, adapted with permission,[89] Copyright 2017, American Chemical Society) and TiO_2 (**CoTpy@TiO_2,** adapted with permission,[91] Copyright 2021, John Wiley and Sons).

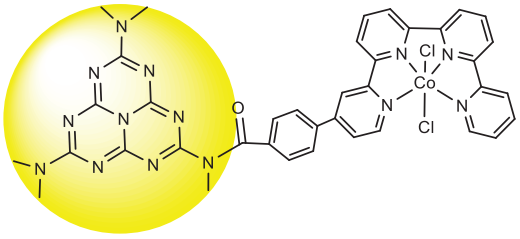

CoQpy@C_3N_4

Scheme 7. CoQpy@C_3N_4 photocatalytic systems for CO_2 reduction. Adapted with permission.[92] Copyright 2020, American Chemical Society.

It has been reported that [Co(**cyclam**)Cl_2]Cl is a highly active CO_2-reduction catalyst when coupled with molecular photosensitizers.[99,100] Matsuoka et al. reported a TON of 54 for CO production from CO_2 reduction for 1 h when using [Co(**cyclam**)Cl_2]Cl as the catalyst and *p*-terphenyl as a photosensitizer (entry 1, **Table 3**).[99] Later, other experiments performed for comparative purposes with heterogenized Co catalysts reported TON in CO of 141.8 (entry 2, Table 3).[102] Nevertheless, [Co^{III}(**cyclam**)Cl_2]Cl is not easy to recycle and its stability under photochemical conditions is low, so great interest has been shown in the last years for preparing and studying heterogenized Co precursors in different supports.

The role of TiO_2 nanomaterials in solar energy conversion is well known. Using Co(III) complexes containing cyclam derivatives as ligands, hybrid photocatalysts have been reported by depositing the Co complex on TiO_2 nanoparticles.[102] Electrons photogenerated in TiO_2 can be transferred to these hybrid Co catalysts for CO_2 reduction. Co catalyst grafted on TiO_2 nanoparticles was prepared by simple deposition using a commercial TiO_2 P25 which consists of 80% anatase and 20% rutile. In this way, **Co^{III}(cyclam)X@P25** (X = Cl or OH) was prepared as a brownish powder refluxing [Co(cyclam)Cl_2]Cl[102] and P25 TiO_2 nanoparticles in acetonitrile containing a small amount of TEA. The heterogenized catalyst could also be obtained by microwave synthesis at 80 °C. In this case, the time for depositing the cobalt complex on TiO_2 surface was shortened from 24 to 2 h. Related complexes **Co^{III}(cyclam)X@SiO_2** are obtained in the presence of silica and the corresponding molecular complexes. The synthesized catalysts were characterized using NMR, FTIR, XPS, and electrochemistry. The FTIR and diffuse reflectance infrared Fourier transform spectroscopy spectra indicate that **Co^{III}(cyclam)X** is in the *trans* configuration, and that Co—O bonds are present in the material suggesting that the deposition of the complex proceeded through the surface hydroxyl groups.

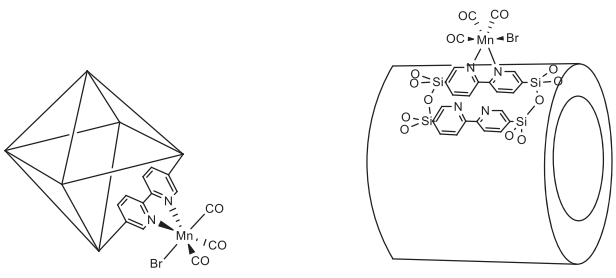

Mn@UiO-67 **Mn@Bpy-PMO**

Figure 9. Mn(I)-Bpyridyl complex incorporated in a UiO-67 MOF (**Mn@UiO-67**) (adapted with permission.[63] Copyright 2015, American Chemical Society) and **Mn@Bpy-PMO** (adapted under the terms of the CC BY-NC 3.0 license.[93] Copyright 2017, The authors, published by Royal Society of Chemistry).

The hybrid **Co^{III}(cyclam)X@P25** material used in photocatalytic CO_2 reduction with TEOA as SD provides CO and H_2 as major products with no significant amount of formic acid observed. Since it is known that Co(**cyclam**) complexes[99,100] as well as P25, produce H_2 under photochemical conditions, the authors proposed that both contribute to the generation of H_2 in photocatalysis with the hybrid material.

A TON of 12.2 was obtained after 4 h using the hybrid **Co^{III}(cyclam)X**@P25 obtained by single deposition on TiO_2 nanoparticles[102] (entry 3, Table 3), while no CO was detected for the mixture of [Co(**cyclam**)Cl_2]Cl and P25 nanoparticles under UV irradiation and small conversion of CO (TON ≈1.3 after 4 h) was produced by a mixture of **Co^{III}(cyclam)X** and P25. When using the photocatalyst prepared by microwave synthesis, a TON of 19.7 was obtained after 4 h (entry 4, Table 3). This enhancement in photocatalytic activity was related to the loading of **Co^{III}(cyclam)X** on the TiO_2 surface. It is observed that hybrid photocatalysts with lower **Co^{III}(cyclam)X** loadings provide higher TONs in CO_2 reduction. Since more **Co^{III}(cyclam)X** was deposited on P25 and anatase by the reflux method than the microwave method, better performances are obtained with the later procedure. However, at high temperatures (100 and 120 °C) the microwave synthesis provides higher loadings of **Co^{III}(cyclam)X** diminishing the photoconversion. Due to the TiO_2 lack of photoresponse in the visible light region, often photosensitizers are used in combination with TiO_2 like for instance **RuBpy** complexes for CO_2 reduction under visible light. In this case, using a Co(III) (cyclam)X/P25 and **RuBpy** under visible-light ($\lambda > 420$ nm irradiation), a TON of 35 for CO production is obtained although the selectivity decreased to CO formation (CO/H_2 ratio = 0.2, entry 5, Table 3).

Following a similar strategy, two different approaches were used for the heterogenization of the Co(III) cyclam catalyst onto mesoporous silica.[103] In the first, [Co(**cyclam**)Cl_2]Cl was covalently attached on SBA-15 by derivatizing one of the amines on the cyclam ring (**[Co(cyclam)Cl_2]@SiO_2**, **Scheme 8**a). The UV-visible spectrum of **[Co(cyclam)Cl_2]@SiO_2** shows a peak around 630 nm characteristic of the *trans* isomer of [Co(**cyclam**)Cl_2]Cl.[101]

In the second approach, the reaction between mesoporous silica and [Co(cyclam)Cl_2]Cl (Scheme 8b) leads to the formation of a brownish powder (**Co^{III}(cyclam)Cl@SiO_2**) by direct reaction of [Co(cyclam)Cl_2]Cl with surface silanol groups (Si—OH) in the presence of TEA.[103] Characterization indicated above shows that in **Co^{III}(cyclam)Cl@SiO_2**, most of the chloride ligand on Co(III) was replaced with O-containing ligands (e.g., –OH and H_2O). The new catalysts were characterized by UV-visible spectra, XPS, and elemental analysis.

The heterogenized Co complexes were tested as photocatalysis in the CO_2 reduction using *p*-terphenyl as PS and a mixture of TEOA and methanol as SD. Under these conditions,

Table 3. Results of CO_2 photoreduction obtained with cyclam-based supported catalysts.

Entry[a)]	Catalyst@Support	Conditions[a)] PS, SD, solvent, lamp, λ nm, t [h]	Main product (TON)[b)]	Selectivity (%, product)	Ref.
1	**$[Co^{III}(cyclam)Cl_2]Cl$**	*p*-terphenyl/TEOA/CH_3OH/CH_3CN (1/1/4 v/v/v / $\lambda > 290$ nm /4 h	CO (54)	$CO/H_2 = 25$	[99,100]
2	**$[Co^{III}(cyclam)Cl_2]Cl$**	*p*-terphenylTEOA/MeOH /CH_3CN (1/1/4) W Hg (100 mW cm^{-2}) 4 h	CO (141.8)	$CO/H_2 = 15.1$	[102]
3	**$Co^{III}(cyclam)X@P25$ X = Cl, OH**[c)]	TEOA/MeOH, $\lambda > 400$ nm/4 h	CO (12.2)	$CO/H_2 = 1$	[102]
4	**$Co^{III}(cyclam)X@P25$ X = Cl, OH**[d)]	TEOA/MeOH, $\lambda > 400$ nm/4 h	CO (19.7)	$CO/H_2 = 1$	[102]
5	**$Co^{III}(cyclam)X@P25$ X = Cl, OH**	**RuBpy**/TEOA/MeOH, $\lambda > 400$/4 h	CO (35)	$CO/H_2 = 0.2$	[102]
6	**$Co^{III}(cyclam)Cl_2@SiO_2$**	*p*-terphenyl TEOA/MeOH/ACN (1/1/4 v/v Hg (100 mW cm^{-2})/4 h	CO (12.5)	$CO/H_2 = 7.8$	[103]
7	**$5Co^{III}(cyclam)X@SiO_2$ X = Cl, OH**	*p*-terphenylTEOA/MeOH/ACN (1/1/4 v/v Hg (100 mW cm^{-2})/4 h	CO (95.5)	$CO/H_2 = 10$	[103]
8	**$20Co^{III}(cyclam)X@SiO_2$ X = Cl, OH**	*p*-terphenyl TEA/MeOH/ACN (1/1/4) W Hg (100 mW cm^{-2})/4 h	CO (160.1, 312)[d)]	$CO/H_2 = 9.8$	[103]
9	**$[Ni(cyclam)]^{2+}$**	**RuBpy**/H_2O/ascorbate (pH 4 or 5), $\lambda > 400$/4 h	CO (4.8)[e)]	100 (CO)	[104]
10	**NiCyCp/RuP**	ascorbate (pH 4) λ 375–79/7 h	CO (15)	n.i.	[105]
11	**NiCycP/RuP@ ZrO_2**	ascorbate (pH 4) λ 375–795, 330, 150 W Xe/7 h	CO (4.8, 7 h) (322, 1 h)	$H_2/CO = 4.15$	[106]
12	**NiCycP@ZnSe**	ascorbic acid (pH 6.5)/MEDA/solar light simulator $\lambda > 400$ nm/4 h	CO (283)	34 (CO)	c

[a)]PS = Photosensitizer, SD = sacrificial electron donor; MEDA = 2-(dimethylamino)ethanethiol; [b)]TON = Turnover number (mols of CO_2 converted/mol catalyst); [c)]Obtained by single deposition on TiO_2 nanoparticles; [d)]Microwave synthesis; [e)]Cumulative amount from repeated irradiation and decreasing loading 1×10^{-4} mol.

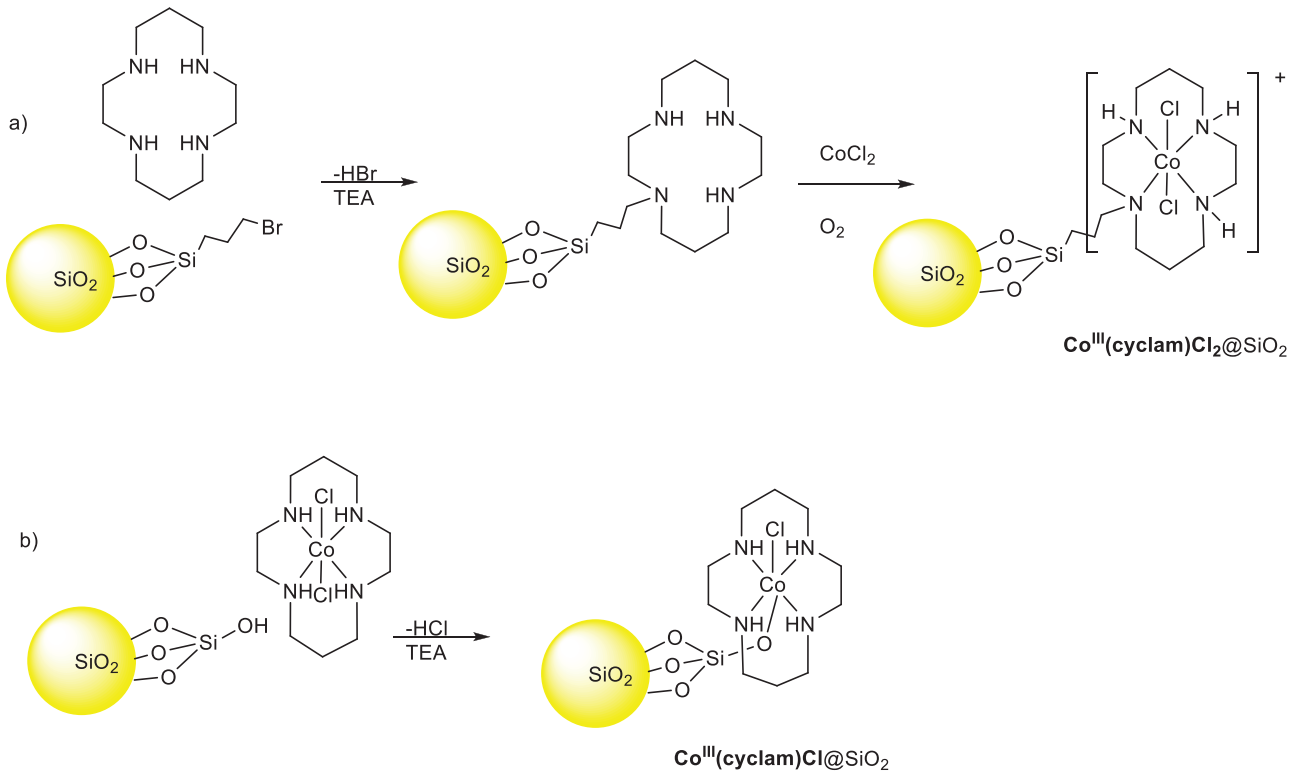

Scheme 8. Synthesis of a) **$Co^{III}(cyclam)Cl_2@SiO_2$** and b) **$Co^{III}(cyclam)Cl@SiO_2$**. Figure based on work by Jin et al.[103]

CO and H_2 were obtained as major products and the formation of formic acid was not significant. **[Co(cyclam)Cl]@SiO_2** shows significantly higher activity as photocatalyst (TON 95.5) toward CO formation than **Co^{III}(cyclam)Cl_2@SiO_2** in photocatalytic CO_2 reduction (TON 12.5) after 4 h. The selectivity toward CO formation, as measured by the CO/H_2 ratio, was determined to be 10 and 9.8 for these two samples (entries 6 and 7, Table 3).

The catalyst loading effect was studied for **Co^{III}(cyclam)Cl@SiO_2** preparing the products with different Co amounts. The CoIII(cyclam)X/SiO_2 samples were synthesized by varying the amount of [Co(cyclam)C_{l2}]Cl (5, 20, and 40 mg) per 200 mg SiO_2 adjusting the corresponding TEOA amount. When the **5Co^{III}(cyclam)X@SiO_2** sample was used as photocatalyst, a TON of 95.5 for CO production was obtained (entry 7, Table 3). The highest activity was achieved using **20Co^{III}(cyclam)X@SiO_2** (entry 8, Table 3) while the selectivity to CO formation decreased as the loading increased. Microwave-assisted heating in the process of supporting the molecular complex to SBA-15 produced a material with uniform distribution of the active centers and enhanced the TON up to 312.[107] Since the same amounts of photosensitizer (*p*-terphenyl) and electron donors (TEOA and methanol) were used in all photocatalytic experiments, increasing the loading of Co(III), the ratio between the concentration of photosensitizer and electron donors to Co(III) decreases, which might influence the CO_2 reduction photocatalyst. Since the Co(III) centers are deposited on the silica surface upon reacting with surface silanol groups, another contributing factor could be related to the Co(III) sites on silica surfaces, which has been studied in detail through different techniques.[103]

In conclusion, in comparison with the molecular catalyst [Co(cyclam)Cl_2]Cl (entry 2, Table 3), the heterogenization via functionalization of silanol groups provides higher productivity in CO_2 photocatalytic reduction.

The interest of the Ni complexes in CO_2 photocatalytic reduction arises from their low cost in comparison to the most studied noble metals. The [Ni(**cyclam**)]$^{2+}$ complex (**Figure 10**) in presence of a molecular photosensitizer such as **RuBpy** photocatalyzed the CO_2 reduction,[104,108] although with very low CO production. Only reducing the nickel **cyclam** concentration to 1×10^{-4} mol L^{-1} and using longer irradiation with replenished sensitizer, a TON of 4.8 for CO was achieved (entry 9, Table 3).

Supramolecular systems consisting of ruthenium polypyridyl complexes covalently linked to [Ni(**cyclam**)]$^{2+}$ have also shown to be active in photocatalytic CO_2 reduction[105] showing the ability of [Ni(**cyclam**)]$^{2+}$ derivatives as catalysts in light-driven processes.

The modification of [Ni(**cyclam**)]$^{2+}$ with a phosphonate linkage allowed to support it to metal oxide surfaces, which are stable in aqueous environments.[106] The Ni(II) **cyclamP** derivative (**cyclamP** = 1,4,8,11-tetraazacyclotetradecan-1-yl)methylene]phosphonic acid) complex was prepared according to the literature[109] providing the novel catalyst [Ni(**cyclamP**)]$^{2+}$. [Ni(**cyclamP**)]$^{2+}$ was immobilized onto ZrO_2 nanoparticles by soaking in an ethanolic solution for 48 h. The successful immobilization in ZrO_2 to form **[Ni(cyclamP)]^2+@ZrO_2** through the phosphonate linkage was confirmed by FTIR and XPS spectroscopies. ICP measurements demonstrated that catalyst is not lost when the heterogenized samples are soaked in aqueous solution (pH 4) confirming the stability of the phosphonate linkage.

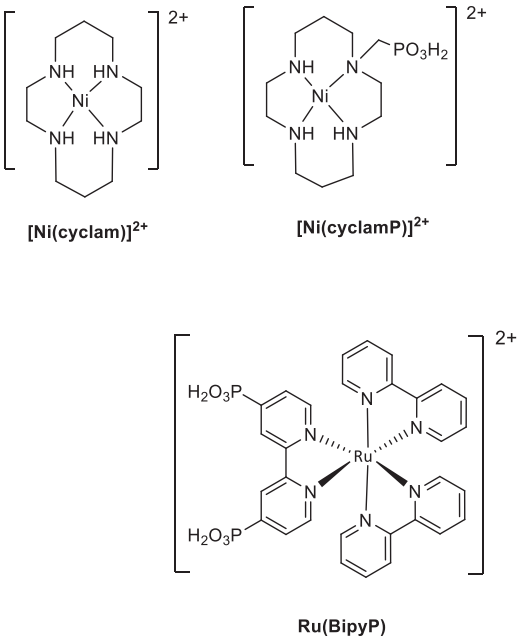

Figure 10. [Ni(**cyclam**)]$^{2+}$ and functionalized [Ni(**cyclamP**)]$^{2+}$ **Ru(BpyP)** structures.

The photocatalytic system was prepared supporting the Ni(II) complex and a Ru-based PS modified with a phosphonic group on ZrO_2. This was obtained by soaking ZrO_2 nanoparticles in ethanolic solutions of **RuBpyP** [Ru(2,2′-bipyridine)$_2$(2,2′-bipyridine-4,4′-diylbis(phosphonic acid))]) and [Ni(**cyclamP**)]$^{2+}$ for 48 h, forming **[Ni(cyclamP)]^2+/RuBpyP@ZrO_2**. The presence of both catalyst and PS supported on the zirconia was confirmed by FTIR, UV-Vis, ICP, and XPS and quantified by ICP analysis. Photocatalytic experiments using **[Ni(cyclamP)]^2+/RuBpyP@ZrO_2** in a CO_2-purged ascorbate buffer (pH 4) under visible illumination provided a relatively high CO evolution rate of 322 mmol g^{-1} h^{-1} corresponding to a TON of 4.8 of CO respect to [Ni(**cyclamP**)]$^{2+}$ after 7 h (entry 10, Table 3). Although the activity decreased for long time periods, probably due to the formation of inactive Ni^I(cyclam)-CO species, the TON in the supported system was higher than the ones reported for homogenous systems like [Ni(**cyclam**)]$^{2+}$ and NiCyCp/RuP, that were 4.8 and 15, respectively (entries 9 and 10, Table 3).[106]

A hybrid system based on a nickel-cyclam complex supported on quantum dots Cd-free such as ZnSe was reported by Reisner and co-workers.[110] To favor the interaction of the Ni complex with the support, the phosphonic acid cyclam derivative was used ([Ni(**cyclamP**)]$^{2+}$, Figure 10). This hybrid system produced mixtures of CO/H_2 with poor selectivity in CO under visible irradiation using ascorbic acid as SD. Interestingly the modification of the surface of the quantum dot with (2-dimethylamino)ethanethiol (MEDA) suppressed part of the H_2 generation enhancing the selectivity to CO (34%) and the TON (283) (entry 12, Table 3).

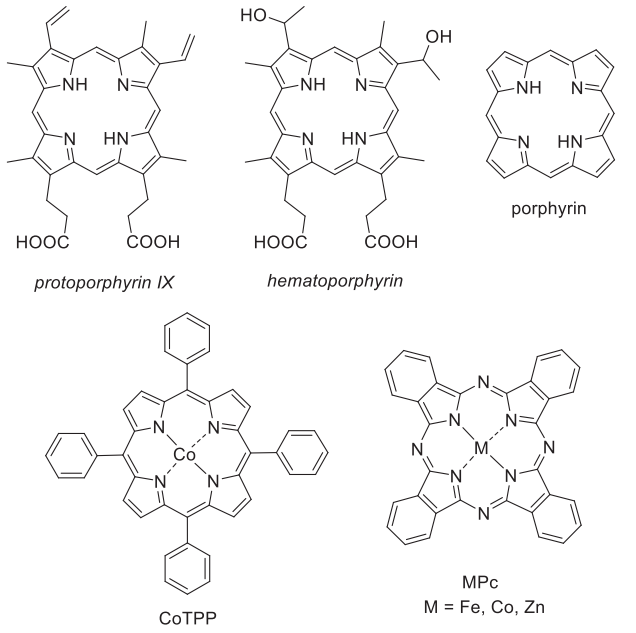

Figure 11. Structures of porphyrins and phthalocyanines adsorbed in Nafion, described in the pioneering work of Ramaraj's group.[112]

5. Tetrapyrrolic Macrocyclic Ligands-Based Photocatalysts

Tetrapyrrolic macrocycles, such as metalloporphyrins and metallophthalocyanines are particularly relevant catalysts for CO_2 photoreduction since they are visible light absorbers with an extended aromatic conjugation, which provides them high molar extinction coefficients and remarkable electron transfer ability. Their aromatic structure can be easily modified and they can form metal complexes with most metallic elements, which allow modulating their physical properties and catalytic activity. In general, the metal centers may exist with oxidation states ranging from +3 to 0, while the macrocyclic framework provides them chemical stability and storage of a reducing equivalent and/or a proton.[111]

One of the first examples of immobilized tetrapyrrolic macrocycle-based catalysts for CO_2 reduction was reported by Ramaraj's group,[112] who described the adsorption of different porphyrins, metalloporphyrins, and metallophthalocyanines (**Figure 11**) onto Nafion membranes (tetrafluoroethylene-based sulfonated polymers) and their evaluation as catalysts in the photoreduction of carbon dioxide to formic acid. The materials were prepared by dipping the Nafion membrane in tetrapyrrolic macrocycle solutions in DMF. After adsorption, the resulting membranes were washed and dried in the dark at room temperature (25 °C). Then, upon dipping the materials in a CO_2 saturated solution and irradiating in the presence of triethanolamine as a sacrificial electron donor, formic acid was obtained as the major product with very high TONs (in the range 10^4). The Nafion membrane support was shown to play a crucial role in the photocatalytic CO_2 reduction system since it imposes a hydrophobic environment around the metalloporphyrin and metallophthalocyanine molecules, which allow them to function selectively as catalysts for CO_2 reduction and not as catalysts for H^+ reduction, which typically takes place predominantly in water. In addition, the authors proposed that highly concentrated tetrapyrrolic macrocycle catalysts in the Nafion membrane may form specific active sites where these photocatalysts are cooperatively involved in CO_2 reduction. This pioneering study demonstrated the importance of the immobilization of the tetrapyrrolic-based photocatalysts in a solid matrix to accomplish a selective multielectron transfer process and paved the way for numerous subsequent works.

It is well established that metalloporphyrins can not only work as light *antennas* as they are extremely able to efficiently adsorb CO_2 from aqueous solutions, and subsequently catalyze CO_2 photoreduction. Moreover, metalloporphyrins' stability can be increased through their effective impregnation into solid supports.

In this section, we describe the most relevant studies regarding the immobilization of porphyrins, chlorins (reduced porphyrin derivatives), and phthalocyanines in solid supports for their application as photocatalysts in CO_2 photoreduction processes. The most significant results are presented in **Table 4**.

An efficient system for the photocatalytic reduction of CO_2 and H_2O was developed by Ohkubo and Fukuzumi's group,[113] which consisted of cobalt(II) chlorin complex **CoChlorin** (**Figure 12**) adsorbed onto multi-walled carbon nanotubes (MWCNTs) as CO_2 reduction catalyst, a $[Ru(II)\mathbf{Me_2phen})_3]^{2+}$ complex as a PS (**Me_2phen** = 4,7-dimethyl-1,10-phenanthroline) and triethylamine as SD, in acetonitrile/water 95:5 v/v. The Co(II) chlorin complex was physically adsorbed on the support simply by mixing and stirring the reaction solution with MWCNTs. Then, the irradiation of a CO_2-saturated acetonitrile solution, containing the system, with visible light, using a xenon lamp with a cut off filter ($\lambda > 420$ nm) at 298 K, resulted in the formation of CO and H_2, with a 2.4 to 1.0 ratio, in high yield (TON up to 710), which was significantly higher than that obtained in the absence of MWCNTs. The good performance of the system was attributed to the π–π interactions between MWCNTs and Co(II) chlorin complex, which were shown to provide a suitable hydrophobic environment for the CO_2 binding instead of a proton (entry 1, Table 4).

Mesoporous materials such as MCM-48 can be also used as supports of metalloporphyrin-based photocatalysts. For instance, Nadeem et al.[114] reported the preparation of copper tetraphenyl porphyrin (**CuTPP**) (Figure 12), impregnated inside the host cages of mesoporous Ti-MCM-48 materials, with different Si/Ti ratios of 100, 50, and 25 (entry 3, Table 4). The impregnation of CuTPP in Ti-MCM-48 was carried out by dissolving the metalloporphyrin in dichloromethane, followed by addition of the Ti-MCM-48 material. The photocatalysts were then tested in the reduction of CO_2 to methanol, where the mesoporous Ti-MCM 48 material with 25 Si/Ti ratio displayed the highest yield (85.88 μmol g^{-1} L^{-1}), when compared with the MCM-48 materials with higher Si/Ti ratios. This result was attributed to the prevalence of Ti^{3+} sites and mid-gap energy states in the material, which results in UV light capturing, followed by the photoexcited electrons selective transfer from the Ti^{3+} sites to the CO_2 molecules adsorbed at the surface (entry 2, Table 4).

Table 4. Results of CO_2 photoreduction obtained with tetrapyrrolic macrocyclic ligands-based supported catalysts.

Entry[a)]	Catalyst@Support	Conditions PS/SD/solvent/λ nm/t [h]	Main product (TON[b)]/TOF[c)]	Selectivity (%, product)	Ref
1	**CoChlorin/@MWCNT**	$[Ru^{II}(Me_2phen)_3]^{2+}$/$Et_3N$/$H_2O$(5%) in MeCN/Xe λ >400 nm /25 h	CO (710)	100 (CO)[f)]	[113]
2	**CuTPP/Ti@MCM-48**	- /0.1 M NaOH, 0.1 M Na_2SO_3/Xe 500 W/0.5 h	CH_3OH (297.06 μmol g^{-1})	100 (CH_3OH)	[114]
3	**CuTPP/Zr@MCM-48**	-/0.1 M NaOH, 0.1 M Na_2SO_3/Xe 500 W/6 h	CH_3OH (193.5 μmol g^{-1})	100 (CH_3OH)	[61]
4	**CuTPP-MOF**	-/TEA/H_2O/Xe 500 W λ > 400 nm /10 min	CH_3OH (262.6 ppm g^{-1} h^{-1})	n.i.	[115]
5	**CoATPP@GO**	methyl viologen/β-NAD, formate dehydrogenase sodium phosphate buffer with TEOA/H_2O/Xe 500 W λ > 400 nm/1 h	HCOOH (96.5 μmol in 2 h)	100 (HCOOH)	[116]
6	**CoTHPP@GO**	-/-/Xe 300 W λ > 400 nm/45 °C/1 h	C_2H_2 (≈112 μmol m^{-2}) CH_4 (≈57.38 μmol m^{-2}	66 (C_2H_2) 34 (CH_4)	[117]
7	**FeTPP@g-C_3N_4**	-/TEOA/MeCN, H_2O (3:1, v:v), Xe 300 W 420 nm <λ < 780 nm/6 h	CO (up to 6)	98 (CO)	[118]
8	**FeTPP@TiO_2**	-/H_2O/ Xe 300 W λ > 420 nm/10 h	CH_4 (20.48 μmol g^{-1} h^{-1})	56.1 (CH_4)	[119]
9	**FeTPP@$CuInS_2$/ZnS**	TEA/4.5 m W Laser λ = 450 nm/10 h	CO (50)	86 (CO) 16 (H_2)	[120]
10	**ZnPc@TiO_2**	– / 0.1 N NaOH aqueous solution/500 W tungsten halogen lamp/25 h	HCOOH (TOF = 320 s^{-1})	75 (HCOOH) 15 (CO) 10 (CH_4)	[121]
11	**CoPc@TiO_2**	– / NaOH aqueous solution/500 W tungsten halogen lamp/10 h	HCOOH (290 μmol g^{-1})	89 (HCOOH) 8 (HCHO) 2 (CH_4) 1 (CH_3OH)	[122]
12	**CuPc@TiO_2**	– / gas phase 45% CO_2, 45% CH_4, 10% He/125 W mercury lamp, 3 h	$HCOO^-$ (14% conversion CO_2) CH_3COO^- (18% conversion CH_4)		[123]
13	**CuPcR@TiO**2	- / NaOH aqueous solution/ HRC UV-VIS lamp 300 W and Xe-Halogen lamp 400 W, 8 h	HCOOH (192 mg l^{-1} g cat^{-1}; 209 μmol g cat^{-1})	100 (HCOOH)	[124]
14	**CoPc-SO**2**NH**2**@GO**	-/TEA/H_2O/ 20 W white cold LED/ 48 h	CH_3OH (3781.9 μmol g^{-1} cat.)	>99 (CH_3OH) 0.82 (CO)	[125]
15	**SnPc@CeO**2**	**SnPc**/Et_3N/DMF, H_2O (3:1)/ 20 W LED λ > 400/24 h	CH_3OH (rate: 97.5 μmol h^{-1} g^{-1}; yield: 2342 μmol g^{-1} cat) CO (rate: 35.0 μmol h^{-1} g^{-1} cat; yield: 840 μmol g^{-1} cat	74 (CH_3OH) 26 (CO)	[126]
16	**CoPc-COOH@g-C_3N_4**	**CoPc-COOH**/Et_3N/DMF, H_2O (3:1)/20 W LED λ > 400 nm/24 h	CH_3OH (yield: 646.5 μmol g^{-1})	100 (CH_3OH)	[56]
17	**CoPPc@mgpCNx**	-/TEOA/CH_3CN/λ > 400 nm/48 h	CO (84)	85 (CO)	[127]
18	**FePc@g-C_3N_4**	-/TEA/MeCN, H_2O (3:1)/ 300 W xenon lamp λ > 400 nm, 12 h	CO (1696.96 μmol g^{-1}) CO (493.35 μmol g^{-1})	100 (CO)	[128]
19	**FePc@g-C_3N_4/PET**	-/TEA/MeCN, H_2O (3:1)/ 300 W xenon lamp λ > 400 nm, 12 h		100 (CO)	[128]

[a]PS = Photosensitizer, SD = sacrificial electron donor, n.i. = not indicated; [b]TON = turnover number ($mol_{product}/mol_{catalyst}$); [c]TOF = turnover frequency ($mol_{CO}/mol_{catalyst}h$); [d]Estimated from TOF reported values; [e]In parallel with H_2 evolution reaction (CO and H_2 were produced with a ratio of 2.4:1); **recycled and reused in five cycles without loss of activity.

The same authors described analogous mesoporous Zr-MCM-48 photocatalyst impregnated also with **CuTPP** (Figure 12), having a Si/Zr ratio of 100, 50, and 25.[61] The Zr-based MCM-48 matrix with maximum Zr content (Si/Zr ratio = 25), possessing a high surface area specific Brunauer, Emmett and Teller of 1324 m^2 g^{-1}, presented the highest photocatalytic activity with 47.5 μmol methanol formation, under UV-visible light irradiation (entry 3, Table 4), which was attributed to efficient photoexcited electron–hole pair separation and transportation to the active Zr^{4+}/Zr^{3+} metal sites from CuTPP, and

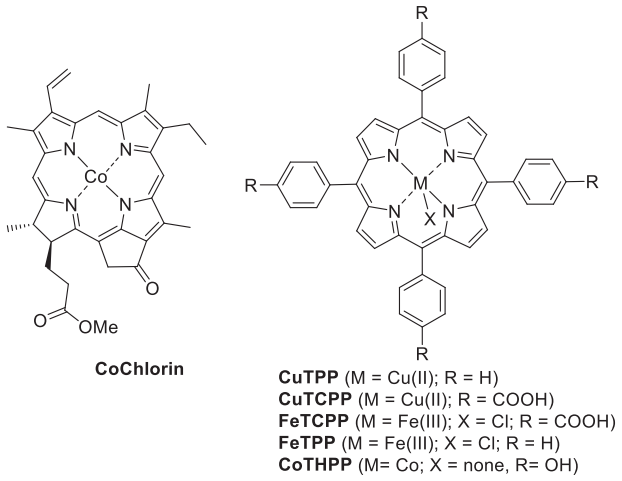

Figure 12. Structures of metalloporphyrin photocatalysts immobilized onto solid supports for CO_2 photoreduction.

also due to the mid-gap energy states formation inside the Zr-MCM-48 material for CO_2 reduction. In addition, the use of 0.1 M Na_2SO_3 was shown to promote a better CO_2 dissolution (with 0.1 M NaOH). Furthermore, light intensity, catalyst concentration, and stirring speed were shown to influence photocatalyst activity toward methanol formation.

Huang and co-workers described a successful photocatalytic reduction process of CO_2 to methanol using an MOF, prepared from 4-carboxyphenyl Cu(II) porphyrin **CuTCPP** (Figure 12).[115] The Cu(II) porphyrin-based MOF was able to promote CO_2 chemical adsorption and was believed to lower the photoreduction barrier, consequently improving the CO_2 reduction efficiency (entry 4, Table 4).

Baeg and co-workers have described the covalent attachment of isatin-porphyrin (IP) chromophore onto chemically converted graphene, which has demonstrated the capability of the photocatalyst/biocatalyst integrated system to promote the selective methanol synthesis from CO_2.[129]

Kumar et al.[116] reported the synthesis of cobalt(II) aminotetraphenylporphyrin (**ATPP**) immobilized onto graphene oxide (**CoATPP@GO**, **Scheme 9**) through treatment of graphene oxide with $SOCl_2$, under reflux, using DMF as the solvent, under an inert N_2 atmosphere, to obtain the appropriately functionalized acyl chloride graphene oxide material, followed by the addition of the cobalt(II) aminoporphyrin (Scheme 9). The resulting nanohybrid was efficiently applied as photocatalyst in CO_2 conversion to formic acid under visible light, presenting a high photosynthetic conversion of 96.49 μmol in 2 h (entry 5, Table 4). The system efficiency was attributed to the vast surface area and the very high carrier mobility of graphene oxide materials, which favor the electrons to be transferred into Co(II) aminoporphyrin. The cobalt hydroxo porphyrin derivative (**CoTHPP**, Figure 12) was used by Niu and co-workers to prepare thin-film photocatalysts on graphene sheets (**CoTHPP@GO**) by spray dispersion over a solid support (quartz or polyethylene terephthalate film).[117] Irradiation of this photocatalyst in CO_2 produced hydrocarbon at a generation rate of about 170.27 μmol m^{-2} h^{-1} as mixtures of acetylene and methane (entry 6, Table 4).

A highly efficient visible-light-driven CO_2 photocatalytic reduction process over graphitic carbon nitride (g-C_3N_4) nanosheets containing tetra(4-carboxyphenyl)porphyrin iron(III) chloride **FeTCPP** was reported by Lin et al. (Figure 12).[118] The g-C_3N_4 nanosheets presented an ultra-thin morphology and the authors hypothesized that such a very thin nature could be beneficial to promote the charge transfer process longitudinally. The higher specific surface area of the g-C_3N_4 nanosheets (135.8 m^2 g^{-1}), when compared with that of bulk g-C_3N_4 (30.0 m^2 g^{-1}), was shown to favor the FeTCPP adsorption. Although the FeTCPP was inactive under visible light irradiation in the absence of g-C_3N_4 nanosheets, the **FeTCPP@g-C_3N_4** heterogenous photocatalysts exhibited an efficient photocatalytic activity for CO_2 reduction to CO, upon visible light illumination (420 to 780 nm), using TEOA as sacrificial reductant, with above 98% selectivity for CO production, only trace amounts of CH_4 and without H_2 or any other products being formed (entry 7, Table 4). Total CO evolution was shown to increase with the increasing amount of porphyrin photocatalyst **FeTCPP (**Figure 12), which was attributed to a higher quantity of catalytic centers. However, the CO yield per gram of **FeTCPP** and the TON value were lower with increasing the amount of **FeTCPP**, due to the fact that **FeTCPP** cannot be fully utilized in case of high excess, which may hinder light harvesting. In addition, the presence of carboxyl groups in the molecular catalysts was also found to be beneficial for the photocatalytic activity, when compared with the analogous nonsubstituted iron(III) tetraphenylporphyrin-based system **FeTPP@g-C_3N_4**, what was attributed to hydrogen bonding between the amino groups at the surface of g-C_3N_4 nanosheets and the carboxyl groups of the iron(III) porphyrin, enhancing the interactions between the photocatalyst and the g-C_3N_4 support and thus, promoting higher electron transfer. Another explanation for that observation is that the **FeTCPP** (having a carboxyl group) is more prone to accepting electrons from the carbon nitride nanosheets, as the E^0 values of Fe(III)/Fe(II)/Fe(I)/Fe(0) redox couples for **FeTCPP** are more positive (or less negative) than those of **FeTPP**, due to the electron-withdrawing nature of the *p*-phenyl carboxyl groups at the *meso* positions of the macrocycle. Based on these results, a plausible mechanism for CO_2 photoreduction over **FeTPP@g-C_3N_4** heterogenous catalysts was proposed (**Scheme 10**), in which the photo-induced electrons in g-C_3N_4 nanosheets are first transferred to **Fe^{III}TCPP** upon irradiation, leading to the formation of the reduced species **Fe^{II}TCPP**. In parallel, the holes left in g-C_3N_4 nanosheets are harvested by the sacrificial reductant agent TEOA. In the presence of CO_2 in solution, the complex intermediate **[Fe^{II}TCPP–CO_2]** is formed, which can further receive electrons from g-C_3N_4 nanosheets (twice) to yield the **[Fe^0TCPP–CO_2]$^{2-}$** species. Then, the catalytically active **Fe^0TCPP** species reduce CO_2 to CO, coupled with proton transfer and, finally, the **Fe^{II}TCPP** species is regenerated, closing the catalytic cycle.

Wu et al. reported an efficient photocatalytic CO_2 reduction with high selectivity for methane formation, using iron (FeTPP, Figure 12) supported on an atomically thin defective TiO_2 material.[119] The **FeTPP@TiO_2** photocatalyst exhibited a CH_4 production rate of 20.48 μmol g^{-1} h^{-1} with a 56.1% selectivity of CH_4 formation, under visible light irradiation (entry 8, Table 4). The oxygen vacancies of defective TiO_2 support were demonstrated

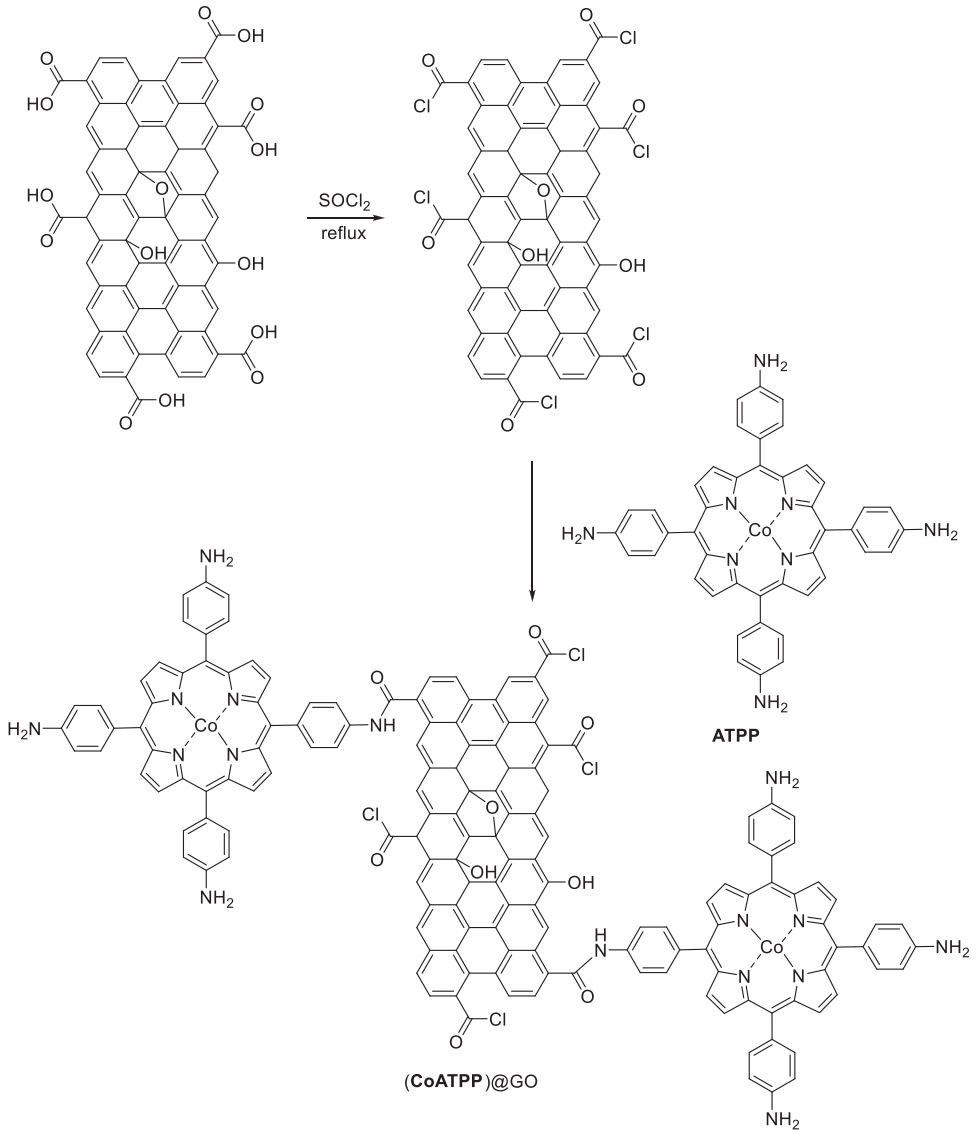

Scheme 9. Synthesis of graphene oxide supported Co(II) aminoporphyrin nanohybrid composite (CoATPP@GO).[116]

to contribute to increasing visible light absorption and simultaneously promote a higher **FeTPP** dispersion. Furthermore, it was shown that FeTPP enhances the adsorption of CO intermediates, thus a synergistic effect between the oxygen vacancies at the solid support and **FeTPP** was found to promote the interfacial charge migration and separation of charge carriers, thus improving the efficiency and selectivity of CO_2 photoreduction to CH_4 (**Scheme 11**).

Quantum dots noble metal-free used as photosensitizers materials to build hybrid systems with **FeTPP** molecular catalyst (**FeTPP@CuInS$_2$/ZnS**) were reported by Lian et al.[120] This hybrid catalyst dispersed in a dimethyl sulfoxide solution produced CO under laser irradiation (λ = 450 nm) achieving a TON of ≈50 with a selectivity on CO of 84% (entry 9, Table 4).

Metallophthalocyanines are chemically stable synthetic molecules, which can be easily prepared and structurally modulated. When compared to porphyrins, the increased π-electrons and the presence of nitrogen atoms in the macrocycle *meso*

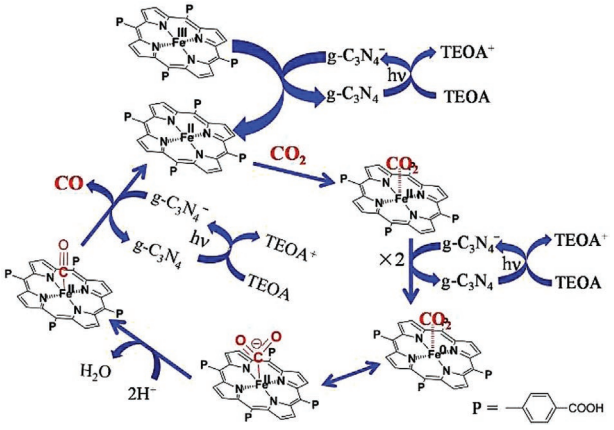

Scheme 10. Proposed catalytic mechanism for CO_2 photoreduction using FeTCPP@ g-C_3N_4 heterogenous catalyst with TEOA as a sacrificial agent. Reproduced with permission.[118] Copyright 2018, Elsevier.

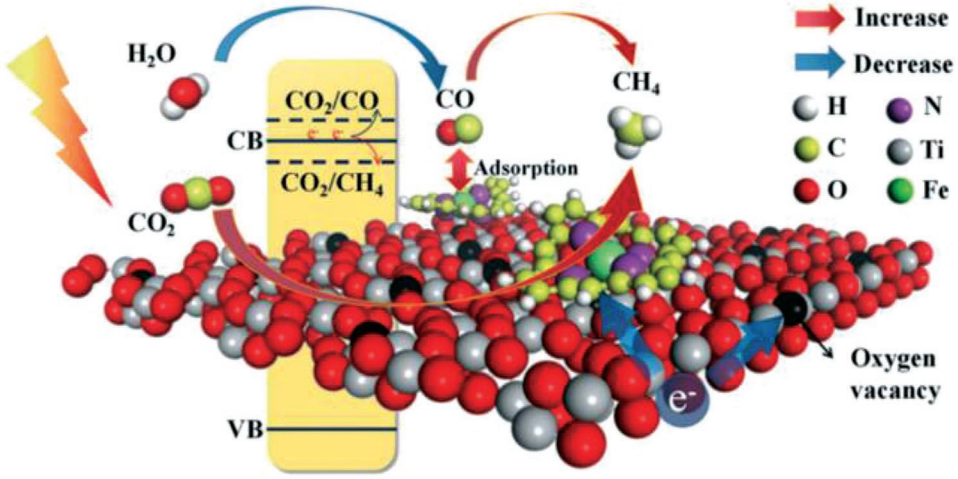

Scheme 11. Schematic diagram of the CO_2 photoreduction to CH_4 mechanism on FeTPP@TiO_2. Reproduced with permission.[119] Copyright 2021, Royal Society of Chemistry.

positions allow the formation of stable metallic complexes and offer intense absorption bands in the near-infrared, in addition to the UV/violet region. Therefore, metallophthalocyanines have been widely studied and used in photocatalytic processes for CO_2 reduction.

Zhao and co-workers described the preparation of zinc phthalocyanine (**ZnPc**)-loaded TiO_2 hybrid material, which was synthesized by a sol–gel method.[121] XRD and differential reflectance spectroscopy techniques clearly demonstrated that **ZnPc** metal complexes (**Figure 13**) were mainly present on the titania surface. Using this hybrid photocatalytic system, carbon dioxide in a NaOH aqueous solution was reduced to produce formate (75%), CO (15%), and CH_4 (10%), using visible light irradiation (entry 10, Table 4). The **ZnPc** was shown to rapidly transfer excited electrons to TiO_2 and enhance the separation of holes and electrons, significantly promoting the photoefficiency. The same authors reported the synthesis of a similar **CoPc**-loaded titania hybrid photocatalyst,[122] which was prepared through an improved sol–gel method, using a homogenous hydrolysis technique. The hybrid material was used in the photoreduction of CO_2 in NaOH solution under ambient conditions, with the formate yield being significantly higher than that of other products, namely, formaldehyde and methanol (entry 11, Table 4).

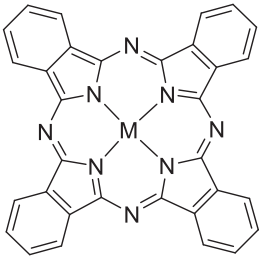

Figure 13. Structures of metallophthalocyanine photocatalysts immobilized onto solid supports for CO_2 photoreduction.

The **CoPc**-loaded titania hybrid material was demonstrated to act as a highly efficient photocatalyst for CO_2 reduction. The photoconductive **CoPc** was able to transfer electron to TiO_2 under irradiation, and capable to reduce the recombination of electron–hole pairs. In addition, OH^- and Na_2SO_3 in aqueous solution were found to be powerful hole scavengers, enhancing the photocatalytic reactivity.

Yazdanpour and Sharifnia reported a copper phthalocyanine (**CuPc**, Figure 13) modified titanium dioxide (**CuPc**@TiO_2) photocatalytic system.[123] The hybrid material was coated on stainless steel mesh and it was applied in the direct photoconversion of carbon dioxide and methane in an appropriate gas-phase batch reactor, under visible light, leading to conversions of 14% and 18% for CO_2 and CH_4, respectively, with the major

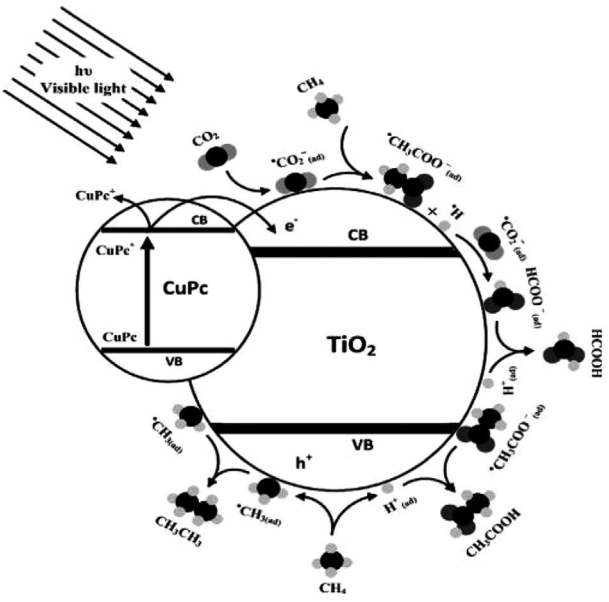

Scheme 12. Diagram of proposed mechanism for CO_2/CH_4 photoreduction with CuPc@TiO_2 photocatalyst. Reproduced with permission.[123] Copyright 2013, Elsevier.

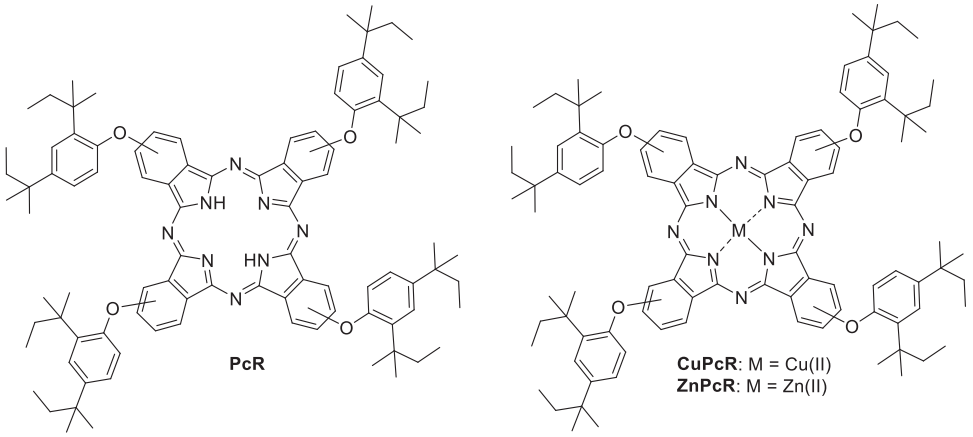

Figure 14. Structures of phthalocyanine photocatalysts immobilized onto TiO_2 for CO_2 photoreduction, reported by Mele et al.[124]

products formed being formate and acetate derivatives (entry 12, Table 4). The authors proposed a mechanistic cycle, which is depicted in **Scheme 12**. Upon irradiation of the **CuPc@TiO$_2$** film with visible light, the **CuPc** is excited to generate an electron in an excited single state of **CuPc** and a hole (h^+) in the ground state of **CuPc**. Then, the electron is injected into the conduction band of TiO_2 and a series of oxidation–reduction reactions occur. The radical $^{\bullet}CH_3$ is produced through CH_4 oxidation by valence band holes, and H^+ are released. Then, two methyl radicals may couple to produce ethane and the conduction band electrons reduce CO_2 to $^{\bullet}CO_2^-$ radicals. $^{\bullet}CO_2^-$ can be attacked by CH_4, and acetate is formed. Then acetate reacts with H^+ to produce acetic acid. If $^{\bullet}CO_2$ radicals are attacked by $^{\bullet}H$, then formate is formed. Finally, the formate may react with H^+, to yield formic acid.

Mele and co-workers described lipophilic metal-free **PcR**, as well as Cu(II)- and Zn(II)tetrakis [4-(2,4-bis-(1,1-dimethylpropyl) phenoxy)]phthalocyanines **CuPcR** and **ZnPcR** (**Figure 14**) loaded over TiO_2.[124] The composite materials were prepared by impregnating TiO_2 (anatase phase) with the desired phthalocyanine-based sensitizers in dichloromethane. The materials were active in the CO_2 photoreduction to formic acid in H_2O, upon irradiation with UV-vis light. Among all, the **CuPcR@TiO$_2$** showed the best catalytic performance (209 μmol g cat^{-1}), exceeding in efficiency other phthalocyanine-based catalytic systems (entry 13, Table 4). In addition, these hybrid photocatalysts presented high chemical stability, and operated under mild reaction conditions (room temperature and moderately acidic pH), avoiding the addition of any organic additives (e.g., radical scavengers) that are usually necessary.

Kumar and co-workers reported graphene oxide-tethered Co(II) phthalocyanine complex **CoPc-SO$_2$NH$_2$@GO** (**Figure 15**).[125] This hybrid composite was used for the photocatalytic reduction of carbon dioxide in water as solvent and triethylamine as the sacrificial donor. It was found that **CoPc-SO$_2$NH$_2$@GO** exhibit high photocatalytic activity (yield = 3781.9 μmol g^{-1} cat; conversion rate = 78.8 μmol g^{-1} cat h^{-1}) with methanol being obtained as the major product (>99%) along with the minor formation of CO (0.82%) (entry 14, Table 4). According to previous literature, the presence of oxy functionalities in the graphene oxide structure creates a 2D network of infinite sp^2 and sp^3 domains, which allows the GO sheet to behave as a semiconductor with valance and conduction bands, thus promoting an efficient photocatalytic activity. Moreover, the catalyst was easily recovered by filtration and reused for the subsequent recycling experiments without significant loss of catalytic activity and selectivity.

The same author also developed heterostructured tin phthalocyanine supported to mesoporous ceria (*meso*-CeO_2).[126] The *meso*-CeO_2 was prepared by combustion method using chitosan as a template. Then, *meso*-CeO_2 was treated with water to enhance the OH groups on the surface and, finally, tin(IV) phthalocyanine dichloride was attached to *meso*-CeO_2 via axial position, through exchange with OH groups of the mesoporous support (**SnPc@CeO$_2$**, **Figure 16**). The hybrid photocatalyst

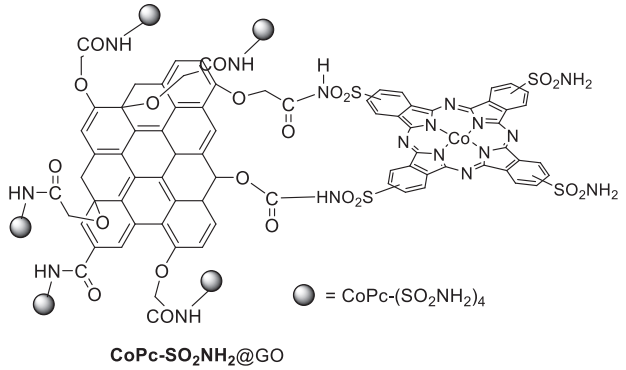

Figure 15. Structure of GO-grafted **CoPc** hybrid photocatalyst.

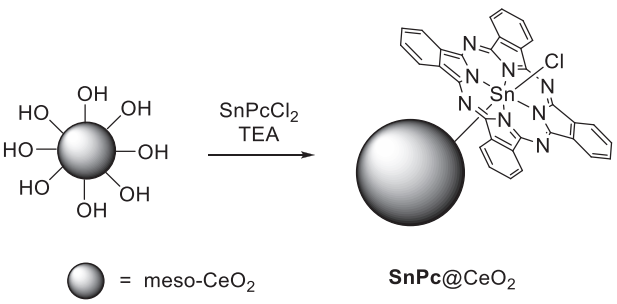

Figure 16. Synthesis of heterostructured tin phthalocyanine supported to mesoporous ceria.[126]

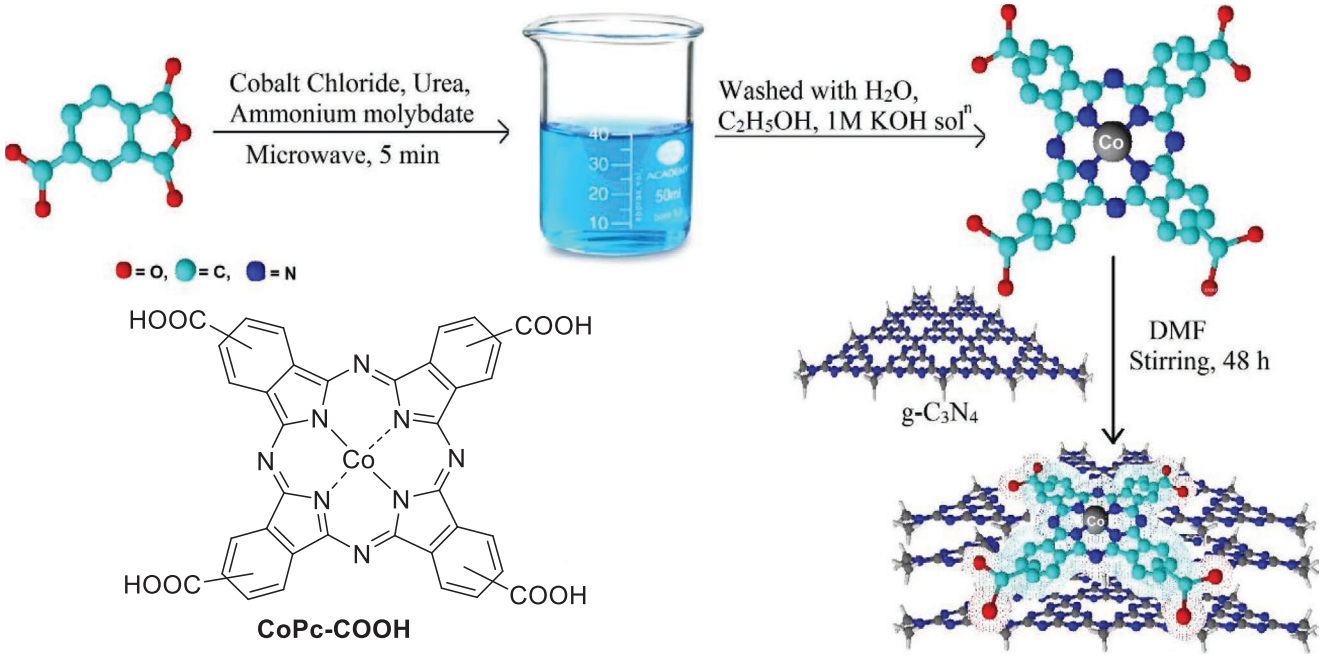

Scheme 13. Synthesis of CoPc-COOH@g-C_3N_4 photocatalyst. Reproduced with permission.[56] Copyright 2019, Elsevier.

SnPc@CeO_2 exhibited good photocatalytic activity under visible light irradiation and afforded methanol and carbon monoxide as major products (entry 15, Table 4), being more efficient than *meso*-CeO_2 and homogenous $SnPcCl_2$. Additionally, the recovered catalyst showed constant catalytic activity for five runs without loss of catalytic activity and selectivity.

More recently, Kumar et al. developed a hybrid photocatalyst consisting of cobalt phthalocyanine tetracarboxylic acid (**CoPc-COOH**) complex immobilized to the organic semiconductor graphitic carbon nitride (g-C_3N_4) (**Scheme 13**).[56] The synthesis of metal complex-semiconductor hybrid photocatalyst was obtained by mixing g-C_3N_4 with **CoPc-COOH** in DMF at room temperature for 48 h under inert N_2 atmosphere. The hybrid material **CoPc-COOH@g-C_3N_4** was found to be a highly efficient photocatalyst for CO_2 reduction to methanol (12.9 mmol g^{-1} cat), using visible light irradiation and triethylamine as sacrificial electron donor (entry 16, Table 4). The catalyst efficiency was attributed to the high CO_2 affinity of the active Co(II) sites, the efficient charge separation/electron mobility due to the g-C_3N_4 surface, prolonged lifetime of the excited state, and high surface area for effective CO_2 conversion. The maximum methanol yield was found 12.9 mmol g^{-1} catalyst, in 24 h irradiation. In addition, the strong interaction between the carboxylic functional groups of **CoPc-COOH** with g-C_3N_4 support heteroatoms makes the hybrid photocatalyst extremely robust, preventing the metal leaching occurrence throughout the photoreduction reactions.

In situ polymerized cobalt phthalocyanine over mesoporous graphitic carbon nitride (**CoPPc@mgp-CNx**, **Figure 17**) was a selective photocatalysts for the reduction of CO_2 to CO. At the optimized Co loading, under full solar spectrum ($\lambda > 300$ nm) in the presence of TEOA/CH_3CN, this material generated 1000 mmol of CO per g after 48 h (TON = 84) with selectivity of 84% which corresponds to a 65% increase compared to that obtained under visible light (entry 17, Table 4).[127] This result confirmed that mgp-CNx acted as the light absorber.

Mo and co-workers reported the synthesis of the **FePc@g-C_3N_4** hybrid catalyst by mixing g-C_3N_4 and **FePc** in refluxing DMF (**Scheme 14**).[128] The **FePc@g-C_3N_4** composite was fully characterized and the scanning electron microscope images confirmed a porous structure consisting of nanosheets with lamellar morphology, showing no significant changes upon loading the metallophthalocyanine complex, which is indicative that the **FePc** molecules are uniformly distributed on the g-C_3N_4 surface. The **FePc@g-C_3N_4** material was applied as photocatalyst in CO_2 reduction, in which g-C_3N_4 works as the

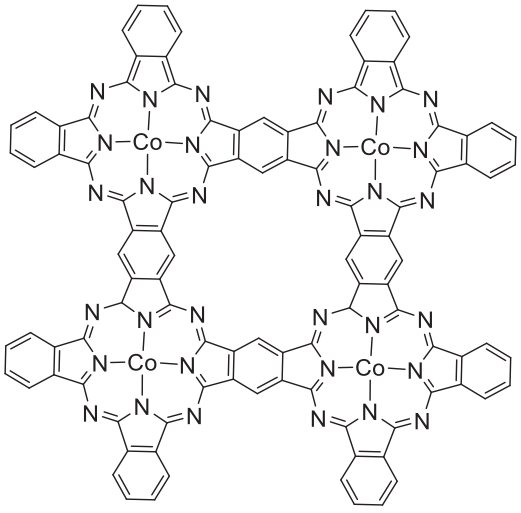

Figure 17. Structures of metallopolyphthalocyanine **CoPPc**.

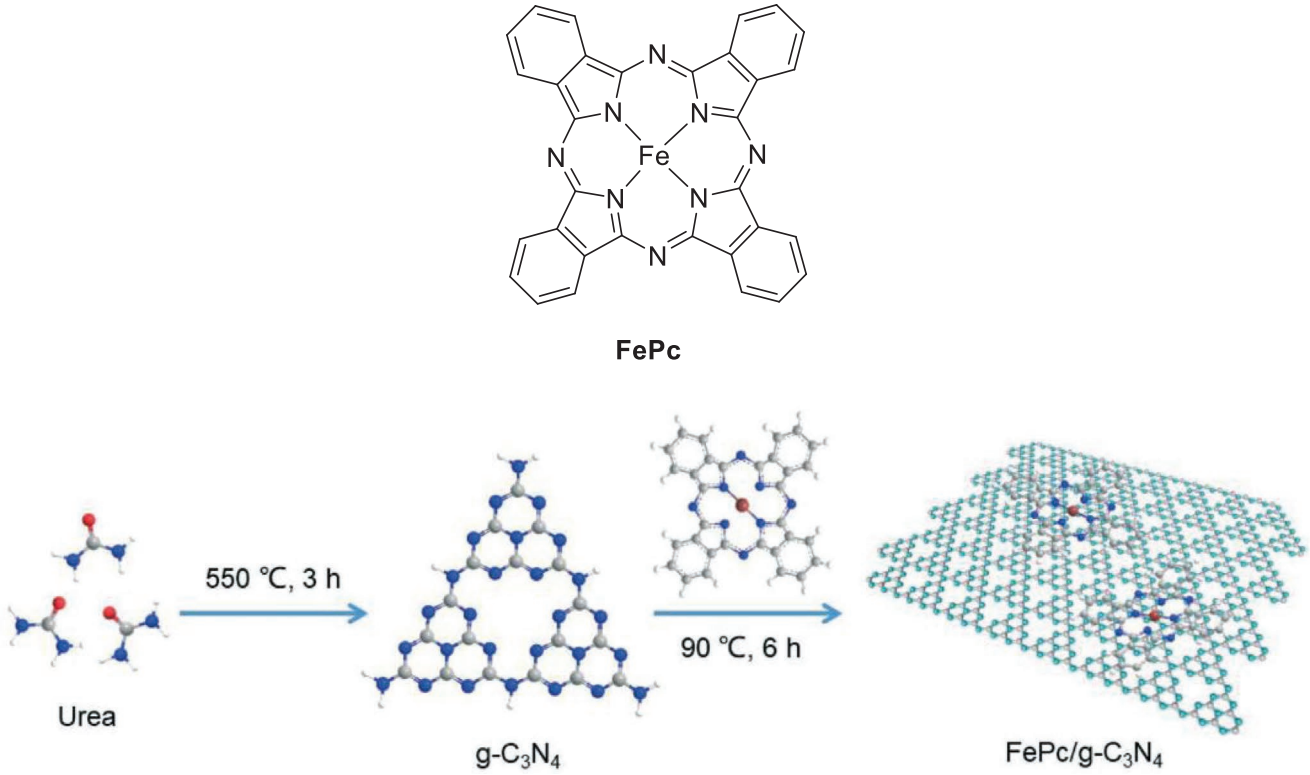

Scheme 14. Synthesis of FePc@g-C_3N_4 photocatalyst. Reproduced with permission,[128] Copyright 2021, Royal Society of Chemistry.

light-harvesting unit while **FePc** acts as the catalytic center. The photocatalytic CO_2 reduction experiments were carried out in a water/acetonitrile system using TEA as a sacrificial reductant agent and visible light. After 12 h irradiation, CO was obtained as a major product (CO yield = 1696.96 μmol g^{-1}), with no liquid products, such as methanol or ethanol, being detected (entry 18, Table 4). Furthermore, inspired by the photosynthesis of natural plants, the authors further immobilized the powder catalysts on polyester (PET) fibers, via a hot-melt adhesive process. Remarkably, the photocatalytic fibers **FePc@g-C_3N_4/PET** catalyst also exhibited high activity for CO_2 reduction to CO (≈490 μmol g^{-1}), under both simulated and natural sunlight, which demonstrates the system's practicability and portability (entry 19, Table 4).

6. Conclusion

The development of efficient CO_2 conversion processes for the production of value-added products is one of the most challenging tasks that the scientific community faces nowadays. Among the various possibilities, photoreduction of CO_2 to generate low valence carbon substances such as carbon monoxide, formic acid, methanol, and methane, has the advantage of using directly the sustainable and practically inexhaustible energy provided by the sun. Nevertheless, this approach presents several challenges. First, efficient, cheap, and available photoactive light-harvesting materials are necessary and active catalysts able to activate CO_2 are also required. So far, the design of molecular catalysts based on metal complexes has produced some interesting examples of photoactive systems for CO_2 reduction. Examples of this are the Re(I) bipyridine-based systems, which are highly selective for the CO_2 to CO photoreduction.[64,65] The low stability and modest activities provided by the examples of the first-generation molecular catalysts have been improved by their combination with solid supports. Thus, using photoactive or photosensitized supports for the Re(I) bipyridine-based systems, the stability was increased and the efficiency was multiplied by ten in terms of TONs for the production of CO.[74,84] Other reduction products can be selectively obtained by changing the metal of the molecular catalyst. For example, ruthenium-bipyridyl-based catalytic systems supported on a combination of graphitic carbon nitride and Ag nanoparticles produced formic acid with high selectivity and efficient quantum yield (5.2%).[50] But to avoid expensive metals, intensive research has been oriented to the development of catalysts formed by complexes of earth-abundant metals such as Co, Ni, Fe, Mn supported on cheap and available solids such as titania, silicon oxides, zirconia, ceria, and carbon-based materials. For example, Co-quaterpyridine[92] and Ni[106] and Co-cyclam[103]-based systems produce mixtures of CO and CO/H_2 with TONs up to 300 in some cases in an aqueous environment. Fe-phthalocyanine supported on graphene nitride produced up to ≈1700 μmol g^{-1}.[127] Selective methanol production has been accomplished using Cu-porphyrin systems.[114,61] Interestingly, the same Fe-porphyrin catalyst produced CO when supported over graphene nitride[118] or methane when supported over TiO_2.[119]

Therefore, these hybrid catalysts have been proved to photocatalyze the reduction of CO_2 at mild conditions selectively to

CO, formic acid, and methanol. Less common has been the eight-electron reduction to methane. Nevertheless, improvements are still required in terms of activities, especially regarding the material photostability and reusability. The combination of the unique reactivity of metallic complexes with CO_2 and the photoactivity and stabilization provided by the supports offer new possibilities in the design of highly active, selective, and reusable catalytic materials. The catalytic activity of these systems of immobilized molecular complexes can be further improved through the modulation of the characteristics of the photosensitizers, the interaction between molecular complex and support, and the electronic properties of the ligands, to tune the parameters involved in intermediate steps of the catalytic cycle such as the light absorption, the proton and electron transfer processes, and the CO_2 reactivity. Selectivity is still the main issue, however hybrid catalysts, in particular photocatalytic conditions, can provide predominantly CO, MeOH, or formic acid depending on the metal and ligand.

Future challenges in the photoreduction of CO_2 should include also the coupling of the CO_2 reduction with oxidation processes leading to useful materials to avoid the generation of residues formed from the sacrificial donors.[91] Finally, it is necessary to develop continuous-flow photoreduction processes with the hybrid materials to avoid deactivation in the semibatch procedures to really assess the stability of the systems.

Acknowledgements

The authors M.R., C.C., and A.M.M.-B. are thankful to the Spanish Ministerio de ciencia e Innovación and AEI/FEDER UE (PID2019-104427RB-100 and PID2020-113187GB-I00), the Departament de Recerca i Univesitats (Generalitat de Catalunya 2017 SGR1472 and 2017 SGR629), and Xarxa d'R+D+I en Química Computacional (XRQTC). R.M.B.C. is thankful to Fundação para a Ciência e a Tecnologia (FCT) and QREN-FEDER for funding through project UID/QUI/00313/2019 (Coimbra Chemistry Centre) and PTDC/QUI-OUT/27996/2017 (DUALPI).

Conflict of Interest

The authors declare no conflict of interest.

Keywords

anchored catalysts, CO_2 reduction, immobilized catalysts, molecular catalysts, photocatalysis, supported catalysts

Received: December 14, 2021
Revised: March 8, 2022
Published online: April 11, 2022

[1] IPCC, *Climate Change 2013–The Physical Science Basis*, Cambridge University Press, Cambridge **2013**.
[2] UN, *Report of the Secretary-General on the 2019 Climate Action Summit and the Way Forward in 2020*, **2019**, https://digitallibrary.un.org/record/3850027 (accessed: January 2022).
[3] T. P. Senftle, E. A. Carter, *Acc. Chem. Res.* **2017**, *50*, 472.
[4] K. M. K. Yu, I. Curcic, J. Gabriel, S. C. E. Tsang, *ChemSusChem* **2008**, *1*, 893.
[5] Q. Liu, L. Wu, R. Jackstell, M. Beller, *Nat. Commun.* **2015**, *6*, 5933.
[6] Y. Tsuji, T. Fujihara, *Chem. Commun.* **2012**, *48*, 9956.
[7] C. Maeda, Y. Miyazaki, T. Ema, *Catal. Sci. Technol.* **2014**, *4*, 1482.
[8] A. M. Appel, J. E. Bercaw, A. B. Bocarsly, H. Dobbek, D. L. Dubois, M. Dupuis, J. G. Ferry, E. Fujita, R. Hille, P. J. A. Kenis, C. A. Kerfeld, R. H. Morris, C. H. F. Peden, A. R. Portis, S. W. Ragsdale, T. B. Rauchfuss, J. N. H. Reek, L. C. Seefeldt, R. K. Thauer, G. L. Waldrop, *Chem. Rev.* **2013**, *113*, 6621.
[9] I. Omae, *Coord. Chem. Rev.* **2012**, *256*, 1384.
[10] T. Sakakura, J.-C. Choi, H. Yasuda, *Chem. Rev.* **2007**, *107*, 2365.
[11] M. Aresta, A. Dibenedetto, A. Angelini, *Chem. Rev.* **2014**, *114*, 1709.
[12] M. Aresta, A. Dibenedetto, A. Angelini, *J. CO2 Util.* **2013**, *3–4*, 65.
[13] M. Aresta, A. Dibenedetto, E. Quaranta, *J. Catal.* **2016**, *343*, 2.
[14] F. D. Rossini, R. S. Jessup, *J. Res. Natl. Bur. Stand. (1934)* **1938**, *21*, 491.
[15] E. Boutin, L. Merakeb, B. Ma, B. Boudy, M. Wang, J. Bonin, E. Anxolabéhère-Mallart, M. Robert, *Chem. Soc. Rev.* **2020**, *49*, 5772.
[16] R. Francke, B. Schille, M. Roemelt, *Chem. Rev.* **2018**, *118*, 4631.
[17] J. L. White, M. F. Baruch, J. E. Pander, Y. Hu, I. C. Fortmeyer, J. E. Park, T. Zhang, K. Liao, J. Gu, Y. Yan, T. W. Shaw, E. Abelev, A. B. Bocarsly, *Chem. Rev.* **2015**, *115*, 12888.
[18] R. Kamata, H. Kumagai, Y. Yamazaki, M. Higashi, R. Abe, O. Ishitani, *J. Mater. Chem. A* **2021**, *9*, 1517.
[19] H. Tian, *ChemSusChem* **2015**, *8*, 3746.
[20] B. Zhang, L. Sun, *Chem. Soc. Rev.* **2019**, *48*, 2216.
[21] K. M. Weyer, D. R. Bush, A. Darzins, B. D. Willson, *BioEnergy Res.* **2010**, *3*, 204.
[22] M. D. Ooms, C. T. Dinh, E. H. Sargent, D. Sinton, *Nat. Commun.* **2016**, *7*, 12699.
[23] N. Kornienko, J. Z. Zhang, K. K. Sakimoto, P. Yang, E. Reisner, *Nat. Nanotechnol.* **2018**, *13*, 890.
[24] J. H. Mussgnug, S. Thomas-Hall, J. Rupprecht, A. Foo, V. Klassen, A. McDowall, P. M. Schenk, O. Kruse, B. Hankamer, *Plant Biotechnol. J.* **2007**, *5*, 802.
[25] J. Jia, L. C. Seitz, J. D. Benck, Y. Huo, Y. Chen, J. W. D. Ng, T. Bilir, J. S. Harris, T. F. Jaramillo, *Nat. Commun.* **2016**, *7*, 13237.
[26] D. K. Dogutan, D. G. Nocera, *Acc. Chem. Res.* **2019**, *52*, 3143.
[27] M. Marszewski, S. Cao, J. Yu, M. Jaroniec, *Mater. Horiz.* **2015**, *2*, 261.
[28] X. Chang, T. Wang, J. Gong, *Energy Environ. Sci.* **2016**, *9*, 2177.
[29] A. Dhakshinamoorthy, A. M. Asiri, H. García, *Angew. Chem., Int. Ed.* **2016**, *55*, 5414.
[30] S. Wang, X. Wang, *Small* **2015**, *11*, 3097.
[31] A. Nakada, H. Kumagai, M. Robert, O. Ishitani, K. Maeda, *Acc. Mater. Res.* **2021**, *2*, 458.
[32] J. A. Maciá-Agulló, A. Corma, H. Garcia, *Chem. – Eur. J.* **2015**, *21*, 10940.
[33] S. N. Habisreutinger, L. Schmidt-Mende, J. K. Stolarczyk, *Angew. Chem., Int. Ed.* **2013**, *52*, 7372.
[34] A. J. Morris, G. J. Meyer, E. Fujita, *Acc. Chem. Res.* **2009**, *42*, 1983.
[35] D. C. Liu, D. C. Zhong, T. B. Lu, *EnergyChem* **2020**, *2*, 100034.
[36] H. Louis, O. U. Akakuru, P. Monday, O. O. Funmilayo, *Eclética Quím. J.* **2019**, *44*, 11.
[37] J. Hawecker, J.-M. M. Lehn, R. Ziessel, *J. Chem. Soc., Chem. Commun.* **1983**, 536.
[38] J. Ran, J. Zhang, J. Yu, M. Jaroniec, S. Z. Qiao, *Chem. Soc. Rev.* **2014**, *43*, 7787.
[39] X. Liu, S. Inagaki, J. Gong, *Angew. Chem.* **2016**, *128*, 15146.
[40] W. Peng, T. H. Chuong Nguyen, D. L. T. Nguyen, T. Wang, T. Van Thi Tran, T. H. Le, H. K. Le, A. N. Grace, P. Singh, P. Raizadaa, M. T. Nguyen Dinh, C. C. Nguyen, S. Y. Kim, Q. Van Le, *Renewable Sustainable Energy Rev.* **2021**, *148*, 111298.

[41] Y. Izumi, in *Advances in CO_2 Capture, Sequestration, and Conversion* (Eds: F. Jin, L.-N. He, Y. H. Hu), ACS Symposium Series, Vol. *1194*, ACS Publication, Washington, DC **2015**, pp. 1–46.
[42] A. J. Cowan, J. R. Durrant, *Chem. Soc. Rev.* **2013**, *42*, 2281.
[43] L. Li, D. Mao, J. Xiao, L. Li, X. Guo, J. Yu, *Chem. Eng. Res. Des.* **2016**, *111*, 100.
[44] S. Cao, J. Low, J. Yu, M. Jaroniec, *Adv. Mater.* **2015**, *27*, 2150.
[45] X. Zhu, C. Tian, G. M. Veith, C. W. Abney, J. Dehaudt, S. Dai, *J. Am. Chem. Soc.* **2016**, *138*, 11497.
[46] Y. Zeng, R. Zou, Y. Zhao, *Adv. Mater.* **2016**, *28*, 2855.
[47] D. D. Zhou, X. W. Zhang, Z. W. Mo, Y. Z. Xu, X. Y. Tian, Y. Li, X. M. Chen, J. P. Zhang, *EnergyChem* **2019**, *1*, 100016.
[48] Y. H. Luo, L. Z. Dong, J. Liu, S. L. Li, Y. Q. Lan, *Coord. Chem. Rev.* **2019**, *390*, 86.
[49] D. Li, H. Q. Xu, L. Jiao, H. L. Jiang, *EnergyChem* **2019**, *1*, 100005.
[50] R. Kuriki, H. Matsunaga, T. Nakashima, K. Wada, A. Yamakata, O. Ishitani, K. Maeda, *J. Am. Chem. Soc.* **2016**, *138*, 5159.
[51] X. Li, J. Wen, J. Low, Y. Fang, J. Yu, *Sci. China Mater.* **2014**, *57*, 70.
[52] M. Aresta, A. Dibenedetto, E. Quaranta, *Reaction Mechanisms in Carbon Dioxide Conversion*, Springer Berlin Heidelberg, Berlin, Heidelberg, **2016**.
[53] A. M. Masdeu-Bultó, M. Reguero, C. Claver, *Eur. J. Inorg. Chem.* **2022**, e202100975.
[54] F. Fang, Y. Liu, X. Sun, C. Fu, Y. Prakash Bhoi, W. Xiong, W. Huang, *Appl. Surf. Sci.* **2021**, *564*, 150407.
[55] P. Kumar, H. P. Mungse, S. Cordier, R. Boukherroub, O. P. Khatri, S. L. Jain, *Carbon* **2015**, *94*, 91.
[56] A. Kumar, P. K. Prajapati, M. S. Aathira, A. Bansiwal, R. Boukherroub, S. L. Jain, *J. Colloid Interface Sci.* **2019**, *543*, 201.
[57] A. Sharma, B. K. Lee, *Catal. Today* **2017**, *298*, 158.
[58] S. Guo, H. Zhang, Y. Chen, Z. Liu, B. Yu, Y. Zhao, Z. Yang, B. Han, Z. Liu, *ACS Catal.* **2018**, *8*, 4576.
[59] K. D. Dubois, H. He, C. Liu, A. S. Vorushilov, G. Li, *J. Mol. Catal. A: Chem.* **2012**, *363–364*, 208.
[60] H. M. Sung-Suh, D. S. Kim, C. W. Lee, S. E. Park, *Appl. Organomet. Chem.* **2000**, *14*, 826.
[61] S. Nadeem, A. Mumtaz, M. S. Alnarabiji, M. I. A. Mutalib, B. Abdullah, *J. Mater. Sci.: Mater. Electron.* **2021**, *32*, 22060.
[62] Y. Li, L. Wen, T. Tan, Y. Lv, *Front. Bioeng. Biotechnol.* **2019**, *7*, 394.
[63] H. Fei, M. D. Sampson, Y. Lee, C. P. Kubiak, S. M. Cohen, *Inorg. Chem.* **2015**, *54*, 6821.
[64] J. Hawecker, J.-M. Lehn, R. Ziessel, *J. Chem. Soc., Chem. Commun.* **1983**, 536.
[65] J. Hawecker, J.-M. Lehn, R. Ziessel, *Helv. Chim. Acta* **1986**, *69*, 1990.
[66] W. Liang, T. L. Church, S. Zheng, C. Zhou, B. S. Haynes, D. M. D'Alessandro, *Chem. – Eur. J.* **2015**, *21*, 18576.
[67] H. Hori, Y. Takano, K. Koike, Y. Sasaki, *Inorg. Chem. Commun.* **2003**, *6*, 300.
[68] C. Liu, K. D. Dubois, M. E. Louis, A. S. Vorushilov, G. Li, *ACS Catal.* **2013**, *3*, 655.
[69] H. Takeda, M. Ohashi, T. Tani, O. Ishitani, S. Inagaki, *Inorg. Chem.* **2010**, *49*, 4554.
[70] S. Zhang, M. Li, W. Qiu, J. Han, H. Wang, X. Liu, *Appl. Catal., B* **2019**, *259*, 118113.
[71] M. Waki, K.-I. Yamanaka, S. Shirai, Y. Maegawa, Y. Goto, Y. Yamada, S. Inagaki, *Chemistry* **2018**, *24*, 3846.
[72] M. Waki, M. Ikai, Y. Goto, Y. Maegawa, S. Inagaki, *Eur. J. Inorg. Chem.* **2021**, *2021*, 1624.
[73] C. D. Windle, E. Pastor, A. Reynal, A. C. Whitwood, Y. Vaynzof, J. R. Durrant, R. N. Perutz, E. Reisner, *Chem. – Eur. J.* **2015**, *21*, 3746.
[74] S.-C. Cui, X.-Z. Sun, J.-G. Liu, *ChemSusChem* **2016**, *9*, 1698.
[75] L. A. Faustino, B. L. Souza, B. N. Nunes, A. T. Duong, F. Sieland, D. W. Bahnemann, A. O. T. Patrocinio, *ACS Sustainable Chem. Eng.* **2018**, *6*, 6073.
[76] M. Wen, K. Mori, Y. Kuwahara, H. Yamashita, *ChemCatChem* **2015**, *7*, 3519.
[77] C. Wang, Z. Xie, K. E. deKrafft, W. Lin, *J. Am. Chem. Soc.* **2011**, *133*, 13445.
[78] H. P. Liang, A. Acharjya, D. A. Anito, S. Vogl, T. X. Wang, A. Thomas, B. H. Han, *ACS Catal.* **2019**, *9*, 3959.
[79] R. Xu, X. S. Wang, H. Zhao, H. Lin, Y. B. Huang, R. Cao, *Catal. Sci. Technol.* **2018**, *8*, 2224.
[80] S. Yang, W. Hu, X. Zhang, P. He, B. Pattengale, C. Liu, M. Cendejas, I. Hermans, X. Zhang, J. Zhang, J. Huang, *J. Am. Chem. Soc.* **2018**, *140*, 14614.
[81] P. Kumar, A. Bansiwal, N. Labhsetwar, S. L. Jain, *Green Chem.* **2015**, *17*, 1605.
[82] K. Maeda, K. Sekizawa, O. Ishitani, *Chem. Commun.* **2013**, *49*, 10127.
[83] D. Sun, Y. Gao, J. Fu, X. Zeng, Z. Chen, Z. Li, *Chem. Commun.* **2015**, *51*, 2645.
[84] Y. Ueda, H. Takeda, T. Yui, K. Koike, Y. Goto, S. Inagaki, O. Ishitani, *ChemSusChem* **2015**, *8*, 439.
[85] Y. Kuramochi, M. Sekine, K. Kitamura, Y. Maegawa, Y. Goto, S. Shirai, S. Inagaki, H. Ishida, *Chem. – Eur. J.* **2017**, *23*, 10301.
[86] K. Sekizawa, K. Maeda, K. Domen, K. Koike, O. Ishitani, *J. Am. Chem. Soc.* **2013**, *135*, 4596.
[87] K. Muraoka, M. Eguchi, O. Ishitani, F. Cheviré, K. Maeda, *J. Energy Chem.* **2021**, *55*, 176.
[88] R. Liu, H. Yoshida, S. Fujita, N. Lu, W. H. Tu, M. Arai, *Appl. Catal., A* **2013**, *455*, 32.
[89] M. F. Kuehnel, K. L. Orchard, K. E. Dalle, E. Reisner, *J. Am. Chem. Soc.* **2017**, *139*, 7217.
[90] Z. Chen, Y. Hu, J. Wang, Q. Shen, Y. Zhang, C. Ding, Y. Bai, G. Jiang, Z. Li, N. Gaponik, *Chem. Mater.* **2020**, *32*, 1517.
[91] E. Lam, E. Reisner, *Angew. Chem., Int. Ed.* **2021**, *60*, 23306.
[92] B. Ma, G. Chen, C. Fave, L. Chen, R. Kuriki, K. Maeda, O. Ishitani, T. C. Lau, J. Bonin, M. Robert, *J. Am. Chem. Soc.* **2020**, *142*, 6188.
[93] X. Wang, I. Thiel, A. Fedorov, C. Copéret, V. Mougel, M. Fontecave, *Chem. Sci.* **2017**, *8*, 8204.
[94] X. F. Zhang, Q. Xi, *Carbon* **2011**, *49*, 3842.
[95] J. L. Wang, C. Wang, W. Lin, *ACS Catal.* **2012**, *2*, 2630.
[96] P. Voyame, K. E. Toghill, M. A. Méndez, H. H. Girault, *Inorg. Chem.* **2013**, *52*, 10949.
[97] R. Kuriki, K. Sekizawa, O. Ishitani, K. Maeda, *Angew. Chem., Int. Ed.* **2015**, *54*, 2406.
[98] S. Matsuoka, T. Kohzuki, C. Pac, S. Yanagida, *Chem. Lett.* **1990**, *19*, 2047.
[99] S. Matsuoka, K. Yamamoto, C. Pac, S. Yanagida, *Chem. Lett.* **1991**, *20*, 2099.
[100] S. Matsuoka, K. Yamamoto, T. Ogata, M. Kusaba, N. Nakashima, S. Yanagida, E. Fujita, *J. Am. Chem. Soc.* **1993**, *115*, 601.
[101] B. Bosnich, M. L. Tobe, G. A. Webb, *Inorg. Chem.* **1965**, *4*, 1109.
[102] T. Jin, C. Liu, G. Li, *Chem. Commun.* **2014**, *50*, 6221.
[103] T. Jin, C. Liu, G. Li, *J. Coord. Chem.* **2016**, *69*, 1748.
[104] J. L. Grant, K. Goswami, L. O. Spreer, J. W. Otvos, M. Calvin, *J. Chem. Soc., Dalton Trans.* **1987**, 2105.
[105] E. Kimura, M. Shionoya, S. Wada, S. Maruyama, X. Bu, *Inorg. Chem.* **1992**, *31*, 4542.
[106] G. Neri, M. Forster, J. J. Walsh, C. M. Robertson, T. J. Whittles, P. Farràs, A. J. Cowan, *Chem. Commun.* **2016**, *52*, 14200.
[107] T. Fenton, S. Gillingham, T. Jin, G. Li, *Dalton Trans.* **2017**, *46*, 10721.
[108] C. A. Craig, L. O. Spreer, J. W. Otvos, M. Calvin, *J. Phys. Chem.* **1990**, *94*, 7957.
[109] S. Füzerová, J. Kotek, I. Císařová, P. Hermann, K. Binnemans, I. Lukeš, *Dalton Trans.* **2005**, 2908.
[110] M. F. Kuehnel, C. D. Sahm, G. Neri, J. R. Lee, K. L. Orchard, A. J. Cowan, E. Reisner, *Chem. Sci.* **2018**, *9*, 2501.
[111] G. F. Manbeck, E. Fujita, *J. Porphyrins Phthalocyanines* **2015**, *19*, 45.

[112] J. Premkumar, R. Ramaraj, *J. Photochem. Photobiol., A* **1997**, *110*, 53.
[113] S. Aoi, K. Mase, K. Ohkubo, S. Fukuzumi, *Catal. Sci. Technol.* **2016**, *6*, 4077.
[114] S. Nadeem, A. Mumtaz, M. Mumtaz, M. I. Abdul Mutalib, M. S. Shaharun, B. Abdullah, *J. Mol. Liq.* **2018**, *272*, 656.
[115] Y. Liu, Y. Yang, Q. Sun, Z. Wang, B. Huang, Y. Dai, X. Qin, X. Zhang, *ACS Appl. Mater. Interfaces* **2013**, *5*, 7654.
[116] S. Kumar, R. K. Yadav, K. Ram, A. Aguiar, J. Koh, A. J. F. N. Sobral, *J. CO_2 Util.* **2018**, *27*, 107.
[117] T. Wu, L. Zou, D. Han, F. Li, Q. Zhang, L. Niu, *Green Chem.* **2014**, *16*, 2142.
[118] L. Lin, C. Hou, X. Zhang, Y. Wang, Y. Chen, T. He, *Appl. Catal., B* **2018**, *221*, 312.
[119] Y. Wu, L. Yan, Y. Yu, C. Jing, *Catal. Sci. Technol.* **2021**, *11*, 6103.
[120] S. Lian, M. S. Kodaimati, D. S. Dolzhnikov, R. Calzada, E. A. Weiss, *J. Am. Chem. Soc.* **2017**, *139*, 8931.
[121] Z. H. Zhao, J. M. Fan, Z. Z. Wang, *J. Cleaner Prod.* **2007**, *15*, 1894.
[122] S. Liu, Z. Zhao, Z. Wang, *Photochem. Photobiol. Sci.* **2007**, *6*, 695.
[123] N. Yazdanpour, S. Sharifnia, *Sol. Energy Mater. Sol. Cells* **2013**, *118*, 1.
[124] G. Mele, C. Annese, A. De Riccardis, C. Fusco, L. Palmisano, G. Vasapollo, L. D'Accolti, *Appl. Catal., A* **2014**, *481*, 169.
[125] P. Kumar, A. Kumar, B. Sreedhar, B. Sain, S. S. Ray, S. L. Jain, *Chem. – Eur. J.* **2014**, *20*, 6154.
[126] P. Kumar, A. Kumar, C. Joshi, R. Singh, S. Saran, S. L. Jain, *RSC Adv.* **2015**, *5*, 42414.
[127] S. Roy, E. Reisner, *Angew. Chem.* **2019**, *131*, 12308.
[128] Y. Mo, C. Wang, L. Xiao, W. Chen, W. Lu, *Catal. Sci. Technol.* **2021**, *11*, 5952.
[129] R. K. Yadav, G. H. Oh, N. J. Park, A. Kumar, K. J. Kong, J. O. Baeg, *J. Am. Chem. Soc.* **2014**, *136*, 16728.

Mar Reguero is a professor of Physical Chemistry at the Department of Physical and Inorganic Chemistry (DPIC) of the Universitat Rovira i Virgili (URV, Tarragona, Spain). Ph.D. in Chemical Sciences (1989), she studied at the Universidad Complutense of Madrid. She worked as a post-doctoral researcher at King's College London, UK, at the Spanish Research Council, Madrid and for Daresbury Laboratory, (UK). In 1993, she enrolled as associate professor at DPIC. Her research in the chemistry field, as a member of the Quantum Chemistry group, is focused on the computational elucidation of mechanisms of photochemical and catalytic reactions.

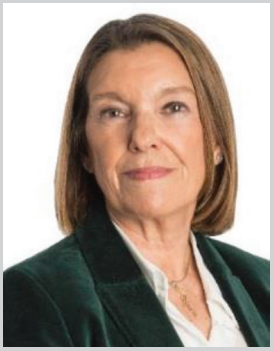

Carmen Claver is a professor of Inorganic Chemistry at URV since 1991 and Emeritus Professor from 2020. Her research focuses on sustainable aspects of catalysis for CO_2 and biomass transformation. She was the Research leader from 1985, Vice-Rector of Research URV (1993–1997), Director of the "Unit of Technology Chemistry" Eurecat (2009–2020). She was recognized as Medal "*Narcis Monturiol*" (2007) from Catalan Government, Chair of excellence *Pierre de Fermat* (Toulouse, France (2009–2011), member of the *Scientific Council* of the CNRS (France, 2009–2014), '*Miguel Catalán-Paul Sabatier*' Price, (*Societé Chimie Française*, 2016), Doctor *"Honoris Causa,"* University Paul Sabatier, Toulouse (2019).

Rui M. B. Carrilho obtained the Ph.D. diploma in Organic Chemistry in 2014 from University of Coimbra (Portugal, 2014) focused on the development of tervalent phosphorus ligands and organometallic compounds for application in catalysis. He was the Postdoctoral researcher in the pharmaceutical *spin-off* Luzitin SA (2014–2015) and at URV (2015–2018). Since 2019, he is an Auxiliary Researcher of the Medicinal Chemistry Group of Coimbra Chemistry Centre and Invited assistant professor at the Chemistry Department of University of Coimbra. His current research interests are mainly focused on the synthesis of P- and N-ligands, metal complexes, and catalyst design for development of catalytic CO and CO_2 activation reactions.

Anna M. Masdeu-Bultó is a professor of Inorganic Chemistry at the Department of Physical and Inorganic Chemistry (URV) since 2020. She obtained the Ph.D. in Chemical Sciences (1992) at the University of Barcelona (Faculty of Chemistry of Tarragona) working on rhodium catalyzed hydroformylation under Prof. Carmen Claver and Aurora Ruiz guidance and pursued postdoctoral research at Ottawa University in Prof. Howard Alper's group (1992). Her research interest has been focused on different aspects of catalysis such as the use of green solvents and carbon dioxide transformation.